Natural Hazards
and Earth System
Sciences

The 2018 west-central European drought projected in a warmer climate: how much drier can it get?

Emma E. Aalbers[1,2], Erik van Meijgaard[1], Geert Lenderink[1], Hylke de Vries[1], and Bart J. J. M. van den Hurk[2,3]

[1]Research & Development Weather and Climate Models, Royal Netherlands Meteorological Institute (KNMI),
P.O. Box 201, 3730 AE, De Bilt, the Netherlands
[2]Institute for Environmental Studies (IVM), Vrije Universiteit Amsterdam, De Boelelaan 1111,
1081 HV Amsterdam, the Netherlands
[3]Deltares, Boussinesqweg 1, 2629 HV, Delft, the Netherlands

Correspondence: Emma E. Aalbers (emma.e.aalbers@gmail.com)

Abstract. Projections of changes in extreme droughts under future climate conditions are associated with large uncertainties, owing to the complex genesis of droughts and large model uncertainty in the atmospheric dynamics. In this study we investigate the impact of global warming on soil moisture drought severity in west-central Europe by employing pseudo global warming (PGW) experiments, which project the 1980–2020 period in a globally warmer world. The future analogues of present-day drought episodes allow for investigation of changes in drought severity conditional on the historic day-to-day evolution of the atmospheric circulation.

The 2018 west-central European drought is the most severe drought in the 1980–2020 reference period in this region. Under 1.5, 2 and 3 °C global warming, this drought episode experiences strongly enhanced summer temperatures but a fairly modest soil moisture drying response compared to the change in climatology. This is primarily because evaporation is already strongly moisture-constrained during present-day conditions, limiting the increase in evaporation and thus the modulation of the temperature response under PGW. Increasing precipitation in winter, spring and autumn limits or prevents an earlier drought onset and duration. Nevertheless, the drought severity, defined as the cumulative soil moisture deficit volume, increases considerably, with 20 % to 39 % under 2 °C warming.

The extreme drought frequency in the 1980–2020 period strongly increases under 2 °C warming. Several years without noticeable droughts under present-day conditions show very strong drying and warming. This results in an increase in 2003-like drought occurrences, compounding with local summer temperature increases considerably above 2 °C.

Even without taking into account a (potentially large) dynamical response to climate change, drought risk in west-central Europe is strongly enhanced under global warming. Owing to increases in drought frequency, severity and compounding heat, a reduction in recovery times between drought episodes is expected to occur. Our physical climate storyline provides evidence complementing conventional large-ensemble approaches and is intended to contribute to the formulation of effective adaptation strategies.

1 Introduction

The impact of recent west-central European droughts and heat waves on society and nature (Vogel et al., 2019; Rösner et al., 2019; Kramer et al., 2019; Schuldt et al., 2020; Beillouin et al., 2020; Bastos et al., 2021; Krikken et al., 2021) once again triggered questions regarding the role of climate change in the occurrence and extremity of drought events (Kornhuber et al., 2019; Yiou et al., 2020; Philip et al., 2020; Zscheischler and Fischer, 2020) and on what to expect under continuing global warming (Toreti et al., 2019; Kornhuber et al., 2019; Hari et al., 2020).

The 2018 growing season was the compound hottest and driest ever recorded in west-central Europe (Toreti et al., 2019; Zscheischler and Fischer, 2020), owing to a sequence of anomalously persistent high-pressure systems over east-

ern, northern and central Europe between April and October (Bissolli, 2019; Sluijter et al., 2018), associated with large-scale atmospheric subsidence, clear-sky conditions, and generally low relative humidity and moisture advection (Sousa et al., 2017, 2018), against the background of globally increasing temperatures (Philip et al., 2020; Vogel et al., 2019). Temperatures were anomalously high over almost the entire European continent (Vogel et al., 2019; Kornhuber et al., 2019), but the precipitation deficit was particularly intense and long lasting in west-central Europe. In this region the deficit built up from April–May until November, only intermittently interrupted by intense but small-scale short-duration rainfall events (Bissolli, 2019; Sluijter et al., 2018). This led to soil desiccation and extremely low groundwater tables (Brakkee et al., 2022) and river discharge (Brunner et al., 2019; Kramer et al., 2019) in the west-central European river basins. The consecutive years 2019 and 2020 were characterized by record-braking heat waves (Vautard et al., 2020; Sousa et al., 2020) and anomalously dry conditions as well (Hari et al., 2020; Bastos et al., 2021; Bissolli, 2020, 2021; Rakovec et al., 2022; Van der Wiel et al., 2023). And again, in 2022, heat waves and severe and particularly widespread drought conditions affected Europe (Toreti et al., 2022). At the time of writing, soil moisture deficits, river water levels and river discharge approached or exceeded 2018 levels in several west-central European river basins, with reported impacts on ecology, agriculture and shipping (Toreti et al., 2022; WMCN-LCW, 2022; BfG, 2022).

Although the probability of heat waves in this region is demonstrated to have increased in response to anthropogenic climate change (Stott et al., 2004; Vogel et al., 2019; Vautard et al., 2020), the attribution of extreme drought events is more complex (Trenberth et al., 2014). Independent drought events are scarce, owing to their long timescale and large spatial scale, which hampers the derivation of robust statistics. Moreover, the processes contributing to widespread drought conditions are not easily disentangled. Intense drought conditions are governed by persistent patterns of atmospheric circulation with low moisture advection into the region of interest. Trends over recent years suggest increases in the frequency and/or persistence of such circulation conditions (Coumou et al., 2014; Kornhuber et al., 2019), but observed circulation-related changes are generally dominated by natural variability (Shepherd, 2014), and there are no significant long-term trends in meteorological (precipitation) drought events in this region (Gudmundsson and Seneviratne, 2016; Hanel et al., 2018; Manning et al., 2019; Spinoni et al., 2019; Philip et al., 2020; Gutiérrez et al., 2021). Nevertheless, observation- and model-based studies find decreasing trends in summer water availability (precipitation minus evaporation) (Spinoni et al., 2019; Padrón et al., 2020) and increases in the frequency and/or severity of soil moisture droughts (Hanel et al., 2018; Philip et al., 2020) as well as in long-duration compound hot and dry events (Manning et al., 2019). This is owing to increasing trends in atmo-

spheric evaporative demand with global warming in the predominantly energy-constrained evaporation regime in west-central Europe.

Under further increasing greenhouse gas concentrations, climate projections agree on a general pattern of year-round decreasing precipitation in the Mediterranean and increasing precipitation in northern Europe, with the drying–wetting transition zone shifting north in summer under higher levels of global warming (Jacob et al., 2014; Aalbers et al., 2018; Coppola et al., 2021; Gutiérrez et al., 2021). For west-central Europe precipitation increases are projected for winter and autumn, while smaller increases or small decreases are projected for spring and summer. Soil moisture is projected to further decrease, with the strongest responses in summer and autumn (Ruosteenoja et al., 2018; Van der Linden et al., 2019), and studies based on large model ensembles show increases in the frequency and severity of (multi-year) drought episodes (Samaniego et al., 2018; Toreti et al., 2019; Hari et al., 2020). The magnitude and direction of the precipitation changes and the magnitude and timing of the soil moisture drying response are uncertain and depend on, e.g., the climate model resolution and generation (Jacob et al., 2014; Coppola et al., 2021; Van der Linden et al., 2019), biases in the mean climate state in the reference period, and the ability of climate models to realistically represent land surface–atmosphere coupling (Orth et al., 2016; Van der Linden et al., 2019; Vogel et al., 2018; Selten et al., 2020) and atmospheric dynamics (Shepherd, 2014; Woollings et al., 2018).

In this study the contribution of global warming to the increase in drought severity and frequency is being addressed by projecting the 2018 drought, as well as the entire 1980–2020 historical period, in a globally warmer world. This is an implementation of the so-called storyline approach (Hazeleger et al., 2015; Shepherd et al., 2018; Shepherd, 2019; Sillmann et al., 2021), a storyline being defined as a "physically self-consistent unfolding of a past events, or of plausible future events or pathways" (Shepherd et al., 2018). Instead of analyzing large-ensemble simulations to derive changes in the probability of extreme drought events, we construct plausible future drought events as analogues of extreme climate events that have actually occurred in the current climate (Hazeleger et al., 2015). As such, changes in droughts in response to global warming can be directly related to real-world events and their societal impact, which make the results very tangible and therewith useful for climate change communication.

Storylines in the form of future analogues of heat waves and droughts have previously been constructed with, e.g., spectral nudging of global climate models (GCMs) (Rasmijn et al., 2018; Wehrli et al., 2020; Van Garderen and Mindlin, 2022) and by selecting events from different warming periods in a very large GCM ensemble (Van der Wiel et al., 2021). Here, we follow a pseudo global warming (PGW) approach (Schär et al., 1996), in which the atmospheric and ocean forcing data of regional climate model (RCM) simu-

lations are perturbed to represent changes in the mean climate state. The PGW method has previously been used – from very simple uniform warming experiments to more advanced perturbations – to examine changes in heavy precipitation (e.g., Attema et al., 2014; Prein et al., 2017; Lenderink et al., 2019), disentangle the contribution of different drivers to amplified Mediterranean warming and drying (Kröner et al., 2017; Brogli et al., 2019), and provide future weather scenarios of extreme precipitation events (Klein Tank et al., 2015; Lenderink and Attema, 2015). In this study, we perform simulations with an RCM forced with reanalysis data to reconstruct the historical period and, specifically, the 2018 drought. For the PGW simulations we essentially rerun the simulations but perturb the atmospheric and oceanic forcing data with climate change information from global climate model (GCM) projections. It has been shown that by perturbing all state variables with the mean climate change signal in GCM projections, a large part of that mean climate change signal is captured (Brogli et al., 2019). At the same time, the day-to-day evolution of the synoptic-scale circulation in the PGW simulations, i.e., the sequence of weather systems entering the model domain, remains essentially determined by the reanalysis forcing and is therefore very similar to the sequence seen in the present-day simulation. Responses from large-scale atmospheric circulation variability are thus suppressed, optimizing the signal-to-noise ratio (De Vries et al., 2022; Lenderink et al., 2023). Another advantage is that the reference climate state, which can have a large impact on drought evolution, is not affected by biases in a GCM since it is based on reanalysis data, thus avoiding one source of uncertainty in future projections.

We focus our analysis on the 2018 drought episode for its recent occurrence and severe impact. Based on the present-day simulations we first explore the atmospheric drivers and soil moisture evolution of the 2018 event under present-day conditions. We repeat this analysis with the PGW simulations, with perturbations derived from three different GCM projections and for several levels of global warming, to diagnose the response in atmospheric drivers, the soil moisture evolution and the severity of the 2018 drought event. Additionally we evaluate the position of this 2018 event in the 1980–2020 period, both for present-day and for future conditions under a single warming level.

The purpose of this work is to provide robust, physically consistent scenarios of what global warming entails for extreme droughts and for the full range of years from wet to moderately dry that occurred in the historical record. It is intended to complement projections of changes in drought risk derived with the conventional large-ensemble approaches, giving an explicit reference to collectively experienced real-world events.

2 Model and methods

2.1 Regional climate model

All simulations are performed with the RCM KNMI-RACMO2 (Van Meijgaard et al., 2012), run at 12 km resolution, with 40 vertical model levels. External forcings for aerosols and greenhouse gases have been implemented according to CMIP5 prescriptions (Collins et al., 2013). RACMO2 uses the land surface scheme HTESSEL (Balsamo et al., 2009), which employs four soil layers with a total depth of 2.9 m. At the bottom of the soil column, boundary conditions are specified as zero heat flux and free drainage. Each land grid cell includes separate tiles for high and low vegetation (16 vegetation types), bare soil, snow on low vegetation/bare soil, snow beneath high vegetation and intercepted water, for which the energy and water balances are solved individually. The tile fractions vary with interception storage and snow cover. The vegetation cover (leaf area index) follows a fixed annual cycle. The model domain is centered over west-central Europe and covers most of Europe.

2.2 Experimental setup

We examine the impact of global warming on the evolution of soil moisture droughts by comparing present-day (REF) and pseudo global warming (PGW) simulations. Table 1 provides an overview of all simulations.

Present-day simulations. The present-day simulations consist of an 11-member initial-condition ensemble covering the period 2018–2020 (2018REF) and a continuous climate simulation covering the period 1980–2017 (climREF). We have created an initial-condition ensemble for 2018–2020 since random small-scale variations in the weather (i.e., due to internal variability within the RCM domain) could otherwise dominate the response. By using an initial-condition ensemble, small-scale variations are sampled, increasing the robustness of the assessment of future changes in a single climate event.

RACMO is run continuously over the period 1 January 1979–1 January 2018, with initial conditions and lateral and sea surface boundary conditions from the ERA5 reanalysis dataset (Hersbach et al., 2020). The sea surface and lateral boundary conditions are updated every 3 h. The first year is used as spin-up, leaving the period 1980–2017 as the reference period for the present-day climate (climREF). The 11-member ensemble for 2018–2020 (2018REF) is created by running RACMO 11 times over the period 2018–2020, reinitializing the atmospheric state to the ERA5 reanalysis on 1 January for member 1, 6 January for member 2 and up to 20 February for member 11. Unless indicated otherwise, throughout this paper analyses for 2018–2020 are based on the ensemble-mean values.

PGW simulations. All simulations are rerun but with perturbed initial land state (soil moisture, soil temperature, snow

Table 1. Model simulations. The data source for the initial land surface conditions (Land surface init.) and the sea surface and initial and lateral atmospheric boundary conditions (Sea & atm. init. & bound.) are indicated. Δ_nK: perturbations for n °C global warming derived from GCM projections, EC: EC-EARTH, HAD: HadGEM2-ES, MPI: MPI-ESM-LR.

| | Period | Start date | Present-day simulations (REF) | | | | PGW simulations ($+n$K$\|GCM$) $n = 1.5, 2, 3; GCM$ = EC, HAD, MPI | | | |
			Name	Member (mb)	Land surface init.	Sea & atm. init. & bound.	Name	Member (mb)	Land surface init.	Sea & atm. init. & bound.
clim	1979-2017	1 Jan 1979	climREF	-	ERA5	ERA5	clim+2K$\|GCM$	-	ERA5 + Δ_{2K}	ERA5 + Δ_{2K}
2018	2018 -2020	1 Jan 2018 6 Jan 2018 ⋮ 20 Feb 2018	2018REF	1 2 ⋮ 11	climREF 2018REF, mb1	ERA5	2018+nK$\|GCM$	1 2 ⋮ 11	2018REF, mb1 + $\Delta_{n\,K}$ 2018+nK$\|GCM$, mb1	ERA5 + $\Delta_{n\,K}$

cover), sea surface (temperature and sea ice extent) and lateral boundary conditions (temperature, humidity, geopotential height and wind). The 2018–2020 simulations are rerun with perturbations consistent with 1.5, 2 and 3 °C global warming with respect to 1991–2020 (2018+nK; $n = 1.5, 2, 3$). We consider different warming levels to examine the sensitivity of the results for 2018 to the level of global warming. The 1979–2017 simulation is rerun with perturbations consistent with a single 2 °C global warming (clim+2K). The clim+2K simulation is used to analyze the 2018 response in the context of climatological changes. Note that the global warming in the 1991–2020 period is 0.9 °C with respect to the 1850–1900 pre-industrial period (HadCRUT v5, Morice et al., 2021). We thus examine the impact of an additional 1.5, 2 and 3 °C global warming, which is projected to be reached within the 21st century under the RCP8.5 (Representative Concentration Pathway) emission pathway in the GCM ensembles described below (see Table A2 for the specific time windows).

The perturbations are determined from the mean climate change signal in three GCM initial-condition ensembles (Tables 1 and A1, described below). For each ensemble, we determine the 30-year period in which the target global warming level with respect to present-day conditions (1991–2020) is reached (Table A2). We then calculate the 3-dimensional monthly-mean climate change signal in the respective 30-year period and add these to the ERA5 sea surface (temperature and sea ice extent) and lateral boundary conditions (temperature, humidity, geopotential height and wind). The initial land state (soil moisture, soil temperature, snow cover) of the clim+2K simulation and member 1 of the 2018+nK ensembles is perturbed with the mean climate change signal in the respective 30-year period at 1 January. The initial land state of member 2–11 of the 2018+nK ensembles is taken from member 1 (as for the present-day simulations).

The physical consistency of the PGW simulations is ensured by perturbing all state variables with a consistent set of perturbations derived from GCM projections. Moreover, the perturbations are (apart from temperature) fairly small and smoothly varying in space and time. In the interior of the RCM domain, simulations are physically consistent by design.

GCMs. Since climate models differ in their regional climate response, we apply perturbations derived from three different GCM initial-condition ensembles: a 16-member EC-EARTH v2.3 (Hazeleger et al., 2010) ensemble produced at KNMI (Royal Netherlands Meteorological Institute), a 4-member HadGEM2-ES (Collins et al., 2011) ensemble and a 3-member MPI-ESM-LR (Giorgetta et al., 2013) ensemble from the CMIP5 archive (Taylor et al., 2012), referred to respectively as EC, HAD and MPI. The perturbations are derived from the ensemble means of the initial-condition GCM ensembles rather than from a single simulation per GCM to obtain a more robust estimate of the climate change signal (Deser et al., 2010; Fischer et al., 2014; Aalbers et al., 2018). All GCM ensembles are run under the RCP8.5 emission scenario. The main characteristics of the three perturbation sets are shown in Appendix A. The simulated global-mean temperature in the reference period in HAD and MPI is fairly close to ERA5 (± 0.1 °C, which is within 1 standard deviation of the annual global-mean temperature; see Table A1). EC has a cold bias of 0.8 °C compared to ERA5. Since we use the GCM simulations only for the derivation of the perturbations (the present-day simulations are driven by ERA5), the impact of the biases in the GCMs is minimized. In the climate response there are large similarities between the three ensembles, all showing the north–south warming and drying gradient, but details like, e.g., the response in the spatial pressure gradient and the shape of the vertical temperature response are different. In terms of regional warming and drying, differences are most pronounced in spring and summer. HAD exhibits the strongest warming in spring; MPI shows the strongest warming and drying in summer.

2.3 Model evaluation

The simulated 2 m temperature and precipitation are evaluated against the gridded observational dataset E-OBS v20.0e and v25.0e (Cornes et al., 2018).

2.4   Indicators and variables

We identify soil moisture drought conditions based on the exceedance of a seasonally varying threshold of the soil wetness index (SWI, -) of the top 1 m of the soil. The top 1 m of the soil is where – in HTESSEL – vegetation has the highest root density and where water deficiencies have the strongest link to agricultural drought (Seneviratne et al., 2012). The SWI is the fraction of plant-available water in the soil, defined as the soil moisture availability (θ, mm) scaled between field capacity (θ_{fc}) and permanent wilting point (θ_{pwp}) (Eq. 1). The SWI is better suited for aggregation over areas with different soil types than θ itself. θ_{fc} and θ_{pwp} are fixed characteristics per grid cell.

$$\text{SWI} = \frac{\theta - \theta_{pwp}}{\theta_{fc} - \theta_{pwp}} \tag{1}$$

A soil moisture drought event is defined as the consecutive period in which the soil moisture conditions are drier than the 5th percentile threshold of the 1980–2017 SWI climatology ($\text{SWI} < \text{SWI}_{5th}$) (Trenberth et al., 2014) for each hydrological year (1 April–31 March) in the 1980–2020 period. SWI_{5th} is calculated for every calendar day based on 14 d smoothed SWI values. We apply the same drought threshold for the present-day and PGW conditions to benchmark the warming-induced changes to present-day conditions. We express the drought severity in terms of the drought deficit volume (D_S, mm d), which integrates drought duration (τ, d) and drought intensity (D_I, mm), comparable to e.g., Yevjevich (1967) and Brunner et al. (2019). It is calculated as the accumulated difference between θ_{5th} and θ over the drought episode (Eq. 2). The analysis is based on a time series with daily values so that the time step Δt in Eq. (2) is 1 d, and the index i varies from the first day ($i = 1$) to the last day ($i = n$) of the drought episode, with $\tau = n$ d. The drought intensity is defined as the drought deficit volume divided by the drought duration (Eq. 3).

$$D_S = \sum_{i=1}^{n} (\theta_i - \theta_{5th,i}) \, \Delta t \tag{2}$$

$$D_I = \frac{D_S}{\tau} \tag{3}$$

In the analyses we use the atmospheric evaporative demand synonymously with potential evaporation (E_p), the evaporation that would take place assuming unconstrained conditions with respect to soil moisture availability and vapor pressure deficit. The computation of evaporation in HTESSEL uses a resistance approach based on Jarvis (1976) for each individual land cover tile (see ECMWF, 2009). To obtain a potential evaporation measure that is fully consistent with the simulated actual evaporation, it is diagnosed in a parallel calculation within RACMO2, using the prevailing atmospheric

conditions but with resistance functions accounting for soil moisture availability and vapor pressure deficit set at a value representing unconstrained conditions. For details, see Appendix B.

2.5   Inter-member variability

The inter-member variability (IMV) of the 2018 ensemble simulations is measured by the standard deviation (σ). The ensemble members of the present-day (2018REF) and PGW (2018+nK) simulations are independent, since the simulations are performed for two separate time slices (opposed to continuous simulations). Therefore, the inter-member variability in the difference between PGW and REF (σ_Δ) is calculated from the standard deviation of the present-day (σ_{REF}) and PGW (σ_{PGW}) simulations.

$$\sigma_\Delta = \sqrt{\frac{\sigma_{REF}^2 + \sigma_{PGW}^2}{2}} \tag{4}$$

2.6   Study area

We focus on the larger river basins in west-central Europe that discharge in the North Sea, namely the Rhine, Meuse, Scheldt, Ems, Weser and Elbe. These river basins are part of the area where the 2018 soil moisture drought episode was most severe and lasted longest, as shown in Fig. 1.

3   The 2018 drought episode in the present-day climate

We first present the main characteristics of the simulated 2018 drought episode and briefly discuss the evaluation of temperature and precipitation against observations. In Fig. 1a maps of the simulated 2018 seasonal anomaly in 500 hPa geopotential height (contours), temperature, precipitation, evaporation and soil moisture are shown for April–June (AMJ), July–September (JAS) and October–December (OND). Anomalies are calculated from 2018 in the 2018REF simulation relative to the 1980–2017 period (climREF). Time series of these variables averaged over the west-central European river basins are shown in Fig. 1b, with observed temperature and precipitation delineated in red. The climatological mean and 5th and 95th percentile thresholds in observed and simulated temperature and precipitation are shown in Fig. C1a.

The 500 hPa geopotential height anomalies in (late) spring (AMJ) and summer (JAS) clearly co-occur with the large positive temperature anomalies and high precipitation deficits (contours and shading in the top two rows of Fig. 1a). Averaged over the west-central European river basins the simulated (observed) temperature anomaly is +3.1 °C (+2.5 °C) over the growing season (April to September), and temperatures exceed the 95th percentile during several episodes. Most noteworthy are 8–22 April, with a 15 d mean temperature anomaly of +6.5 °C (+6.0 °C), and
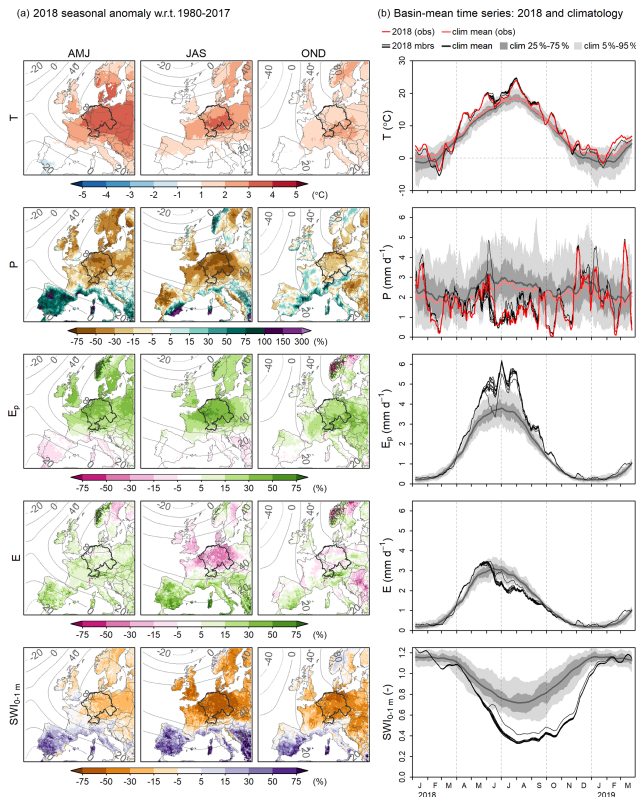
Figure 1. The 2018 drought episode. **(a)** Maps of the simulated seasonal-mean anomaly with respect to 1980–2017 in 500 hPa geopotential height (contours, m) and (top to bottom) near-surface temperature (T), precipitation (P), potential evaporation (E_p), evaporation (E) and the top 1 m soil wetness index ($\mathrm{SWI}_{0\text{-}1\,\mathrm{m}}$), for April–June (AMJ), July–September (JAS) and October–December (OND). Data are masked over sea for visibility. The west-central European river basins are marked in black. **(b)** Time series of the simulated basin-mean (top to bottom) temperature, precipitation, (potential) evaporation and top 1 m SWI for January 2018–March 2019 and the 1980–2017 climatology. Thin black lines show the individual 2018REF ensemble members (mbrs). The thick grey line and dark- and light-grey shading depict respectively the 1980–2017 mean and 25th–75th and 5th–95th percentiles. Observed (E-OBS v20.0) temperature and precipitation are shown for 2018 (red line) and the 1980–2017 mean (pale-red line). Time series are smoothed with a 14 d running mean.

22 July–8 August, with an 18 d mean anomaly of $+5.9\,^\circ\mathrm{C}$ ($+5.1\,^\circ\mathrm{C}$). The latter period was indeed classified as a heat wave in the individual countries (Yiou et al., 2020; Sluijter et al., 2018; Vogel et al., 2019; Bissolli, 2019). Apart from a cold bias in winter, the basin-mean simulated absolute temperatures are fairly accurate, with a small underestimation with respect to the observed 1980–2017 mean temperature in the growing season ($-0.3\,^\circ\mathrm{C}$) and overestimation of the extreme conditions of 2018 temperatures ($+0.3\,^\circ\mathrm{C}$) in most members of the 2018REF ensemble.

Basin-mean precipitation is anomalously low in each month from February to November. Averaged over the growing season, the simulated (observed) basin-mean precipitation anomaly is $-1.1\,\mathrm{mm\,d^{-1}}$ or $-41\,\%$ ($-37\,\%$), with the largest, basin-wide deficits in June ($-56\,\%$ ($-43\,\%$)) and in July ($-64\,\%$ ($-64\,\%$)). Mean precipitation is overestimated compared to the observations with on average $0.2\,\mathrm{mm\,d^{-1}}$, both for the climatology and 2018.

Under prevailing conditions of clear skies, high solar radiation, high temperatures and increasingly dry air, the response in the atmospheric evaporative demand is substantial ($+1\,\mathrm{mm\,d^{-1}}$ or $+35\,\%$ over the growing season). Also the actual evaporation is anomalously high from April until the beginning of June, modulating the near-surface temperatures. However, it cannot keep up with the rise in atmospheric evaporative demand, owing to quickly increasing soil and canopy resistance against evaporation in response to decreasing relative humidity and soil moisture availability and has below-normal values from mid-June to October. As a consequence, the sensible heat flux strongly increases (not shown), which corresponds to an amplified rise in summer and autumn near-surface temperatures. Averaged over the growing season, the actual evaporation is slightly smaller than normal ($-0.1\,\mathrm{mm\,d^{-1}}$ or $-6\,\%$).

The resulting extremity of the 2018 soil moisture drought is clearly reflected (bottom row of Fig. 1). Anomalously low soil moisture levels occur in large parts of central and northern Europe, but, consistent with the persistent precipitation deficits, conditions are most severe and persistent in west-central Europe. Averaged over the west-central European river basins the soil moisture conditions are around normal at the start of the growing season, owing to low temperatures and evaporation in March. Soils steadily deplete from April onwards, reach severely dry conditions (exceeding the 5th percentile) in the second half of May and are lowest in early August. Soil moisture levels remain very low throughout the growing season up to the end of October. This is when precipitation starts to exceed the evaporation and soil moisture replenishes, reaching the 5th percentile threshold in the beginning of January 2019, after nearly 8 months of severely dry conditions. By then, the soil moisture deficit volume has accumulated to 8240 mm d, with a mean drought intensity of 36 mm. In Sect. 5.1 and Fig. 6 we will show the extremity of this number compared to other drought episodes in the 1980–2020 period. Normal soil moisture levels in the top 1 m of the soil are reached by early February 2019. For deeper soil layers the winter precipitation is insufficient to fully replenish the soils to normal levels, and the anomalously dry conditions persist throughout 2019 (see Fig. C1b).

The overestimation of precipitation could imply an overestimation of the soil moisture levels. On the other hand, the overestimation of the 2018 summer temperature likely leads to a dry bias in soil moisture. The amount of inter-member spread in the 2018REF ensemble (natural variability generated within the RCM model domain) is found to

be considerable in some periods, as seen in Fig. 1b (dark shading). The spread is largest in the period from the end of May to early June when variability in the location and intensity of precipitation-bearing systems induces relatively strong variability in wetness and temperature. While the ensemble spread in temperature is relatively short lived, the ensemble spread in soil moisture reduces more slowly over summer. One ensemble member receives much higher precipitation amounts in May–early June, as well as in July and August. Evaporation in this member is consequently relatively high throughout summer, and the temperature is 1.1 °C (June) to 0.3 °C (September) lower than the ensemble mean, closer to the observations. Apart from model biases and natural variability, differences between actual and simulated atmospheric and soil conditions are possibly related to interactions between soil moisture and groundwater in especially the low-lying coastal areas, which are not taken into account in HTESSEL.

4 Response to pseudo global warming

4.1 Climatological-mean response to 2 °C warming

We next present the climatological-mean response to a 2 °C warming to provide context to the 2018 response. Figure 2 shows the seasonal response patterns in geopotential height, near-surface temperature, precipitation, (potential) evaporation and soil moisture over Europe for the EC-perturbed simulations. The annual cycle in the basin-mean response in these and additional variables is shown in Fig. 3. Results for the HAD- and MPI-perturbed simulations can be found in Appendix D.

The spatial response patterns exhibit the well-known seasonally varying warming and drying gradients over Europe (e.g., in the EURO-CORDEX ensemble (Coppola et al., 2021) and the RACMO–EC-EARTH initial-condition ensemble (Aalbers et al., 2018), showing that the PGW simulations indeed capture the main characteristics of the full climate response (Brogli et al., 2019; De Vries et al., 2022). In spring, autumn and winter the warming gradient is oriented roughly northwest–southeast, with the weakest warming over the British Isles and coastal regions adjacent to the Atlantic Ocean and North Sea (blue colors represent warming below 2 °C). In summer, warming ranges between around 2.0 °C over Scandinavia to around 3.0 °C, locally 3.5 °C in southern Europe. Averaged over the river basins the near-surface temperature response varies between +1.4 °C in May and +2.6 °C in August (black line in Fig. 3a). Note that the interannual spread around the 1980–2017 mean response (grey box and whiskers) is rather large, especially in JAS, which will be discussed in Sect. 5.2.

The transition zone of increasing precipitation in the north and decreasing precipitation in the south is positioned just southwest of the west-central European river basins in spring
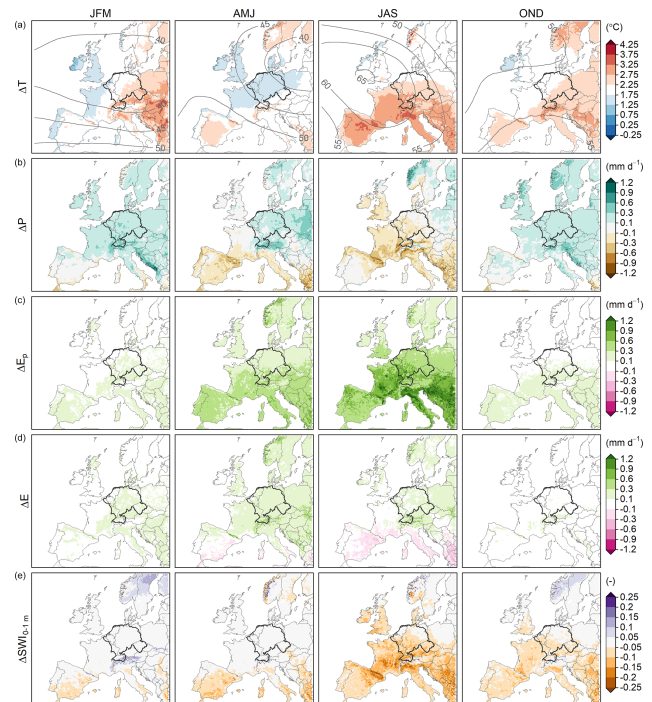
Figure 2. Climatological-mean response (1980–2017) to 2 °C warming in **(a)** the geopotential height at 500 hPa (contours) and near-surface temperature (T, shading), **(b)** precipitation (P), **(c)** potential evaporation (E_p), **(d)** evaporation (E), and **(e)** the top 1 m soil wetness index ($SWI_{0-1\,m}$), averaged over January–March (JFM), April–June (AMJ), July–September (JAS) and October–December (OND). Results are based on climREF and clim+2K|EC.

and autumn and over the northeast of the basins in summer, yielding increasing precipitation in winter, autumn and early spring and small decreases in summer for the basin mean (Figs. 2b, 3e). This co-occurs with nearly constant relative humidity in late autumn, winter and early spring and decreases in relative humidity in JJASO (June–October; Fig. 3d). Net surface solar radiation increases in JJASO (Fig. 3b), when cloud cover and relative humidity decrease. Under conditions of higher temperatures and enhanced by the increase in solar radiation and decrease in relative humidity from late spring to late autumn, the atmospheric evaporative demand increases over land throughout the year (Figs. 2c, 3f). The present-day soil moisture regime in west-central Europe allows for year-round increases in actual evaporation in almost all years, with around the potential rate in winter and early spring but smaller than the potential rate in JJASO (Figs. 2d, 3g), resulting in increases in the sensible heat flux in the latter period (Fig. 3c).

For the combined river basin area, the increased evaporation and reduced summer precipitation lead to enhanced soil moisture depletion in late spring and summer, while in autumn and winter increases in precipitation result in a faster soil moisture replenishment. This feature of the response
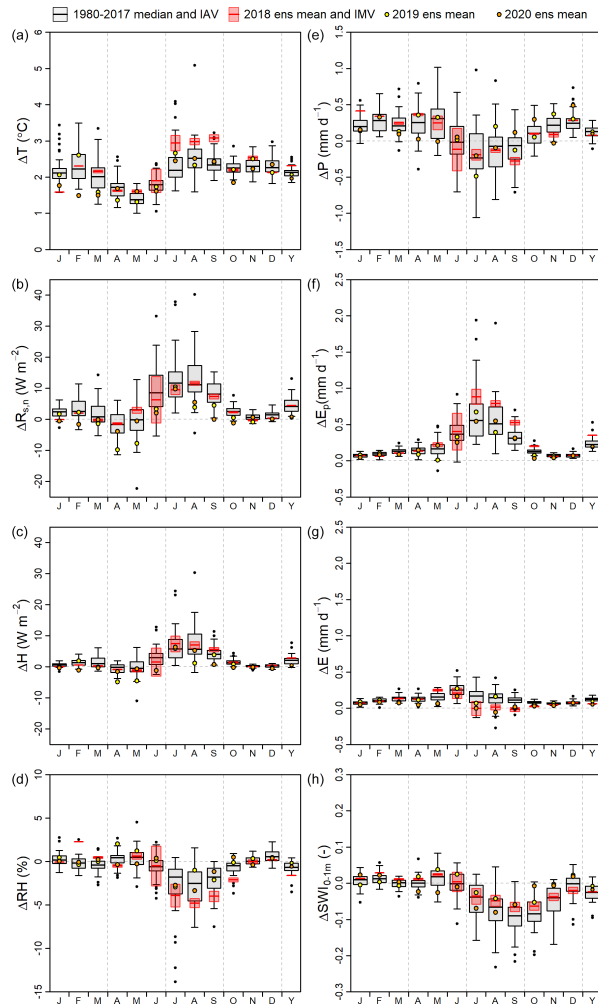
Figure 3. Annual cycle in the basin-mean response to 2 °C global warming for 1980–2017 and the individual years 2018–2020, for the EC-perturbed simulations in **(a)** near-surface temperature (T), **(b)** net solar radiation at the surface ($R_{s,n}$), **(c)** sensible heat flux (H), **(d)** near-surface relative humidity (RH), **(e)** precipitation (P), **(f)** potential evaporation (E_p), **(g)** actual evaporation (E) and **(h)** the top 1 m SWI. The monthly (J–D) and annual (Y) response to 2 °C warming are calculated for each year. Boxplots show the median (black bar) and inter-annual variability (IAV) of the response for the years 1980–2017, depicting the interquartile range (box), the total range with a maximum distance of 1.5 times the interquartile range outside the box (whiskers) and outliers (black dots). The red bars and box delineate the ensemble mean and inter-member variability (IMV, mean ±1 standard deviation (σ_Δ)) of the response for 2018. The yellow and orange dot depict the 2019 and 2020 ensemble-mean response.

is amplified by a larger fraction of precipitation falling as rain in autumn (due to higher temperatures) and reduced snowmelt in spring (due to a smaller snowpack). The resulting soil moisture levels in the top 1 m of the soil are around present-day or even wetter conditions in winter and early spring but drier from mid-June to December, with a maxi-

mum drying response in September (Figs. 2e, 3h). In summer and autumn, the soil moisture availability in deeper layers and runoff decrease as well (see Fig. D3). However, the response in annual precipitation equals the response in annual evaporation, meaning that each winter soil moisture levels in all layers are restored to present-day levels and decreases in summer runoff are compensated by increases in winter.

With the amplitude of the response and the position of the drying–wetting transition zone being dependent on the GCM, the MPI- and HAD-perturbed simulations give slightly different results (see maps in Figs. D1 and D2 and time series in Figs. D4 and D5). The drying–wetting transition zone is located further northeast in all seasons for both clim+2K|MPI and clim+2K|HAD. clim+2K|MPI shows a weaker temperature response in spring but much stronger warming and drying in JAS (Fig. D1a, b), consistent with a strong response in the geopotential height anomaly (contours in Fig. D1a). The soil moisture depletion over the growing season in the west-central European river basins is consequently stronger but so is the soil moisture replenishment in autumn and winter (Figs. D1e, D4i). clim+2K|HAD shows a stronger temperature and evaporation response in spring than the EC- and MPI-perturbed simulations, increases in precipitation are overall smaller, and soil moisture levels are found to decrease earlier in spring (Figs. D2, D5).

4.2 2018 response to 2 °C warming

The response of the hot and exceptionally dry growing season of 2018 that unfolded under persistent conditions of atmospheric blocking is shown for the basin mean in Fig. 3 (red boxes). Maps of the 2018 response anomaly with respect to the climatological-mean response are shown in Fig. 4 for 2018+2K|EC. Results for 2018+2K|HAD and MPI can be found in Appendix D.

The 2018 response in winter and early spring preceding the blocking conditions is very similar to the climatological-mean response in most variables and results in slightly wetter soil moisture conditions at the start of the growing season in April in 2018+2K|EC than in 2018REF. Also in spring, the 2018 soil moisture and circulation anomalies do not have a strong effect on the response. Consistent with the climatological-mean response, precipitation is found to increase in April and May, with relatively strong increases in April. Apparently, the precipitation events originate from sources with sufficient moisture supply to sustain these increases. Note that the precipitation response is rather patchy (Fig. 4b), despite the application of the 11-member ensembles. Evaporation rises by more than the potential rate in these months but only partially compensates the precipitation increase. Despite a small decrease in snowmelt and increase in runoff (see Fig. 5b; discussed in Sect. 4.3), the top 1 m of the soil is slightly wetter until mid-June in 2018+2K|EC than in 2018REF.
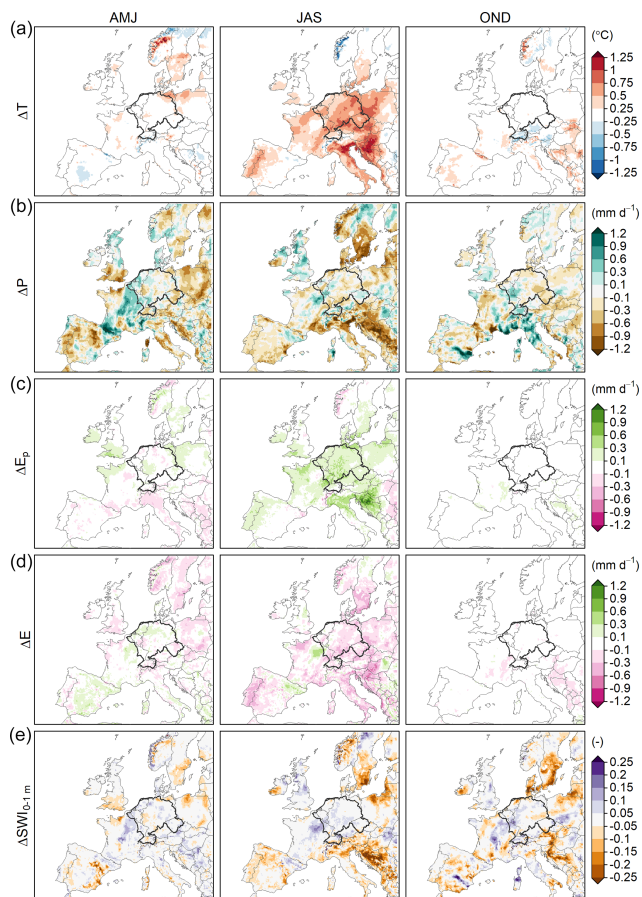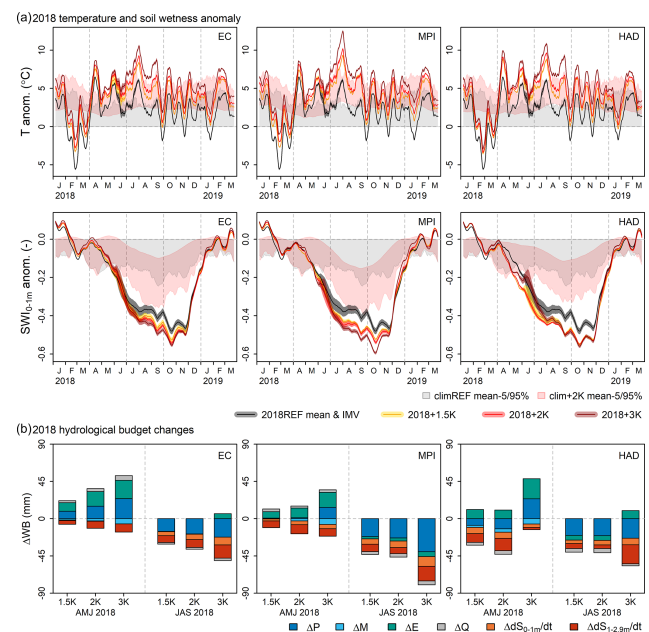
Figure 4. Difference between the 2018 and climatological-mean (1980–2017) response to 2 °C warming $(2018+2\,\mathrm{K}|\mathrm{EC}-2018\mathrm{REF}) - (\mathrm{clim}+2\,\mathrm{K}|\mathrm{EC}-\mathrm{climREF})$ in **(a)** temperature, **(b)** precipitation, **(c, d)** (potential) evaporation and **(e)** the SWI in the top 1 m of the soil.

Figure 5. Impact of global warming on the 2018 near-surface temperature (T), soil wetness ($\mathrm{SWI}_{0-1\,\mathrm{m}}$) and the hydrological budget (WB), for the EC- (left column), MPI- (middle) and HAD-perturbed (left) simulations. **(a)** Time series of the basin-mean anomaly in the 2018 T and $\mathrm{SWI}_{0\text{-}1\,\mathrm{m}}$ with respect to the present-day climatology for present-day (grey line and shading), 1.5 °C (orange), 2 °C (red) and 3 °C (brown) global warming. Shading indicates the inter-member variability (IMV) as in Fig. 3. For reference, the 1980–2017 mean − 5th–95th percentile envelope for present-day (pale-grey shading) and +2 °C (pale-red shading) conditions is shown as well. **(b)** Change in the hydrological budget over the 2018 AMJ and JAS periods in response to 1.5, 2 and 3 °C global warming. The hydrological budget is given by $\mathrm{d}S_{0-1\,\mathrm{m}}/\mathrm{d}t + \mathrm{d}S_{1-2.9\,\mathrm{m}}/\mathrm{d}t = P + M - E - Q$, with $\mathrm{d}S_{0-1\,\mathrm{m}}/\mathrm{d}t$ and $\mathrm{d}S_{1-2.9\,\mathrm{m}}/\mathrm{d}t$ being the seasonal change in soil moisture storage in respectively the top 1 m of the soil and bottom soil layer and the seasonally integrated fluxes of precipitation (P), snowmelt (M), evaporation (E) and runoff (Q). Note that $\mathrm{d}S/\mathrm{d}t$ is negative over AMJ and JAS (soil moisture depletion) so that a negative response of $\Delta\mathrm{d}S/\mathrm{d}t$ corresponds to an increase in soil moisture depletion under global warming, as can be seen in the bottom row of **(a)**.

From mid-June onwards strong deviations from the climatological-mean response occur for the temperature, relative humidity, atmospheric evaporative demand and evaporation responses, exceeding the 25th–75th percentile range of 1980–2017 (Figs. 3a, d, f, g and 4a, c, d). Decreases in precipitation (June–September) and the weak evaporation response (July–September) show that sources of moisture are even more limited in a 2 °C warming scenario. Precipitation in this period originates from predominantly continental sources (Benedict et al., 2021), and the evaporation response is moisture constrained throughout Europe (Fig. 4c, d).

From July to September the temperature response over the basin area and surroundings is amplified compared to the climatological-mean response (+3.0 °C over the 2018 JAS period compared to +2.4 °C for the climatology in the basin area). This response anomaly correlates with the anomalously low response pattern of actual evaporation. Within the basin, evaporation barely increases or even decreases in the period July–October and co-occurs with a further decrease in

relative humidity, a modest increase in the sensible heat flux (Fig. 3c) and an increase in near-surface temperature. Note that the increase in solar radiation is relatively small in June and July (Fig. 3b), given the predominantly clear-sky conditions in 2018REF, and that the increase in the sensible heat flux is only slightly larger than the climatological response. Increases in heat advection due to stronger warming in up-wind regions or enhanced warming through subsidence may play a role in the amplified warming as well.

Since the response in summer evaporation in the west-central European river basins is close to zero, the JAS soil moisture response is small compared to most other years in the 1980–2020 period (Fig. 3h) and is almost completely de-

termined by the decrease in precipitation. The pattern of the soil moisture response anomaly strongly correlates with the precipitation response anomaly in this period (Fig. 4e). Percolation to deeper soil layers and runoff decrease in this period as well (see Figs. D3 and 5b; discussed in Sect. 4.3). In autumn and winter, moderate precipitation increases replenish the soils to 2018REF levels in December–January in the top 1 m of the soil and in deeper layers.

4.3 Sensitivity of the 2018 response to the level of global warming and GCM perturbations

In Fig. 5 we show the 2018 basin-mean time series of the anomaly in near-surface temperature, the top 1 m SWI (Fig. 5a) and the hydrological-budget changes over AMJ and JAS (Fig. 5b) for all warming levels and PGW simulations (EC, MPI and HAD).

In the EC-perturbed simulations, the temperature response is fairly linear with global warming under the increasingly moisture-constrained conditions, with 2.2, 3.0 and 4.3 °C warming during the July–August heat wave under respectively 1.5, 2 and 3 °C global warming and 1.7, 2.3 and 3.4 °C warming for the growing-season mean. This yields temperature anomalies during the July–August heat wave (i.e., deviations with respect to climREF) of +8.1, +8.9 and +10.2 °C, compared to +5.9 °C under present-day conditions. The soil moisture depletion over the growing season increases with higher levels of global warming but only from mid-June onwards. In AMJ, precipitation increases are stronger under 3 °C warming than under 1.5 °C but so are the evaporation increase, snowmelt decrease and runoff increase, resulting in the almost zero change in soil moisture depletion in the top 1 m of the soil over AMJ for higher levels of global warming. The increase in soil moisture depletion over JAS for higher levels of global warming is mainly driven by stronger decreases in JAS precipitation. Although the JAS evaporative demand increases with higher levels of global warming, actual evaporation does not increase or only does so very weakly. Note that the soil moisture depletion in deeper soil layers is more pronounced and occurs throughout the growing season (red bar in Fig. 5b).

In the MPI-perturbed simulations for 2018, the soil moisture response is fairly similar to the EC-perturbed simulations in spring, despite a weaker increase in AMJ precipitation, which is compensated by a weaker increase in evaporation. Also in summer and autumn the soil moisture drying is fairly similar under 1.5 and 2 °C warming, as is the response in hydrological-budget terms. Under 3 °C warming the soil moisture drying is more pronounced owing to a stronger decrease in precipitation. JAS evaporation decreases, and the JAS temperature response is amplified compared to 1.5 and 2 °C warming.

The HAD-perturbed simulations under 1.5 and 2 °C warming give a stronger near-surface heating and show soil moisture drying from the start of the growing season onwards.

This is a feature of the climatological-mean response under 2 °C warming (solid red line in Fig. 5a; see Sect. 4.1), but it is more pronounced under the circulation of 2018. In contrast to the EC- and MPI-perturbed simulations and the HAD-perturbed simulations under 3 °C warming, precipitation decreases in AMJ. Under 3 °C warming, the response in the hydrological-budget terms is fairly similar to the EC-perturbed simulations, yet the response in the near-surface temperature is stronger.

5 Impact on drought and heat

5.1 Drought severity and frequency

To further quantify the impact of global warming on drought occurrences and severity in the west-central European river basins under 2 °C warming, we determine the basin-mean drought deficit volume, duration and intensity for all years in the 1980–2020 period under present-day and +2 °C conditions (Figs. 6 and D8). Under present-day conditions, the severity of the 2018 drought episode clearly stands out in both duration and intensity. Next in line is the 2003 drought episode, which has comparable duration but smaller mean intensity than 2018 and is indeed known for its severe hot and dry conditions and associated societal and economic impacts in central Europe (e.g., Rebetez et al., 2006; Fischer et al., 2007). Furthermore, the 2011 spring drought (Trachte et al., 2012) and the 2020 drought (Bissolli, 2021; Rakovec et al., 2022) are noteworthy. The 2019 soil moisture drought severity (Bissolli, 2020; Rakovec et al., 2022) is in reality likely more similar to the 2020 drought event. Comparison with observations (E-OBS) shows an underestimation of the simulated precipitation deficit in the 2019 growing season, while in the 2020 growing season the precipitation deficit is overestimated in most members and the temperature anomaly is somewhat higher than observed (Fig. C1b).

Under 2 °C warming the drought frequency strongly increases compared to present-day conditions, reflecting the on average drier soil moisture conditions in summer and autumn. However, the drought response is highly non-linear, and several drought episodes emerge that exceed the historic 2003 drought severity. 2018 is still the most severe drought in the 1980–2020 period under 2 °C warming, but the deviation from other years decreases; 1983, 1989 and 2020 are more similar to 2003 under 2 °C warming. The frequency of droughts exceeding the present-day 2003 episode more than doubles, occurring on average once every 8 years. This is found for all PGW simulations, irrespective of the GCM supplying the perturbations, although the response in drought intensity in the PGW simulations based on +2K|MPI is generally stronger than for the other two GCMs.

For 2018, the drought onset and ending under global warming occur at roughly the same time as for the present-day event in +2K|EC for all warming levels, with only small
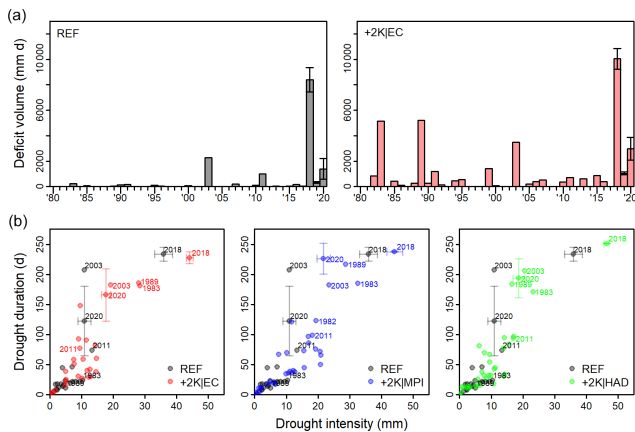
Figure 6. Impact of $2\,°C$ warming on drought severity in 1980–2020, expressed as **(a)** the soil moisture deficit volume and **(b)** the drought duration and intensity. Shown is the annual maximum drought per hydrological year (April–March) under reference (grey) and $+2\,°C$ conditions for the EC-perturbed simulations (red) in **(a)** and for reference (grey) and each of the PGW simulations of EC (red), MPI (blue) and HAD (green) in **(b)**. Error bars show the ensemble mean ± 1 standard deviation for 2018–2020. For some members the 2020 drought is split into two consecutive drought episodes, which explains the large inter-member spread (see Fig. C1b).

differences between the individual members (Fig. 5a). The drought duration is thus hardly affected compared to REF, while the drought intensity shows a 23 % increase (44 mm in $+2$K|EC compared to 36 mm in REF), resulting in a 20 % increase in the drought deficit volume under $2\,°C$ warming (Fig. 6). The drought onset in $+2$K|MPI and $+2$K|HAD occurs somewhat earlier than in $+2$K|EC, and the increase in drought deficit volume is stronger ($+25\,\%$ or $+39\,\%$ under $2\,°C$ warming). Under $1.5\,°C$ global warming the increase in the 2018 drought deficit volume is slightly smaller, while a larger intensity and deficit volume are simulated under $3\,°C$ warming (EC and MPI) with the tendency of shorter drought episodes owing to springtime precipitation increases (all simulations). Table D1 summarizes the findings for all warming levels and GCMs.

The increase in drought severity is surprisingly strong for the years 1983 and 1989. Under present-day conditions, 1983 and 1989 were not marked as severe drought periods in most parts of the study area (see Fig. 7, where we present the basin-mean soil moisture evolution and spatial drought structure in JAS for the top five future droughts for present-day and $2\,°C$ warming). Yet, under the specific circulation conditions in 1983 and 1989, the globally warmer climate background results in strongly reduced precipitation, increased evaporation (1983 only) and soil drying in spring and early summer, a very strong response in incoming solar radiation, a negative response in evaporation, and very strong increases in the sensible heat flux and near-surface temperatures later

in summer (see also the next section). The outliers in Fig. 3 correspond to these years.

The large spatial extent of all future drought analogues is remarkable (Fig. 7b). A much larger part of Europe is affected than under present-day conditions. The drought expansion is not limited to southern Europe, where climatological soil moisture drying is largest. The 2018 event, for instance, spreads in all directions, now also covering southern Sweden, Poland and the Baltic states.

5.2 Co-occurring dry and hot conditions

As we have seen for the present-day 2018 drought event, the extremely dry conditions co-occur with extremely high temperatures, and while the soil moisture response to 1.5, 2 and $3\,°C$ global warming is fairly modest, the local temperature response is amplified compared to the mean climate response, especially in JAS (Fig. 3). The co-occurrence of the JAS basin-mean SWI and near-surface temperature under present-day and $+2\,°C$ conditions for all years in the 1980–2020 period is shown in Fig. 8 for $+2$K|EC, along with the co-occurrence of the response in these variables. The present-day T–SWI distribution generally shifts towards warmer and drier conditions under $2\,°C$ warming, with larger inter-annual variability in both variables (Fig. 8a). Strong responses in soil moisture drying (1983, 1989) co-occur with particularly strong temperature increases, but some years with small soil moisture responses (2003, 2018) also exhibit fairly strong warming (Fig. 8b), which contributes to an increase in inter-annual variability in both temperature and soil wetness. The increase in inter-annal variability is somewhat less pronounced in the HAD-perturbed simulations (see Fig. D9).

The non-linearity in the drying and warming response is related to the transition of predominantly energy-limited to more moisture-limited evaporation in west-central Europe (Schär et al., 2004; Lenderink et al., 2007; Seneviratne et al., 2010; Zscheischler and Seneviratne, 2017). Years with weakly moisture-limited evaporation under present-day conditions (showing relatively small differences between actual and potential evaporation; see E and E_{p} in Fig. 1b) may shift to strongly soil-moisture-limited energy balance regimes under PGW, through a decrease in precipitation and enhanced early-season evaporation. Conversely, several years with present-day JAS temperature and soil wetness comparable to 1989 and 1983 show a much weaker response. The specific large-scale circulation (variability) and in particular the corresponding precipitation response are important factors in the initiation of soil moisture drying and amplified warming. However, the drought evolution is unique for each year, and disentangling the exact drivers of the amplified drying response is outside the scope of this paper.
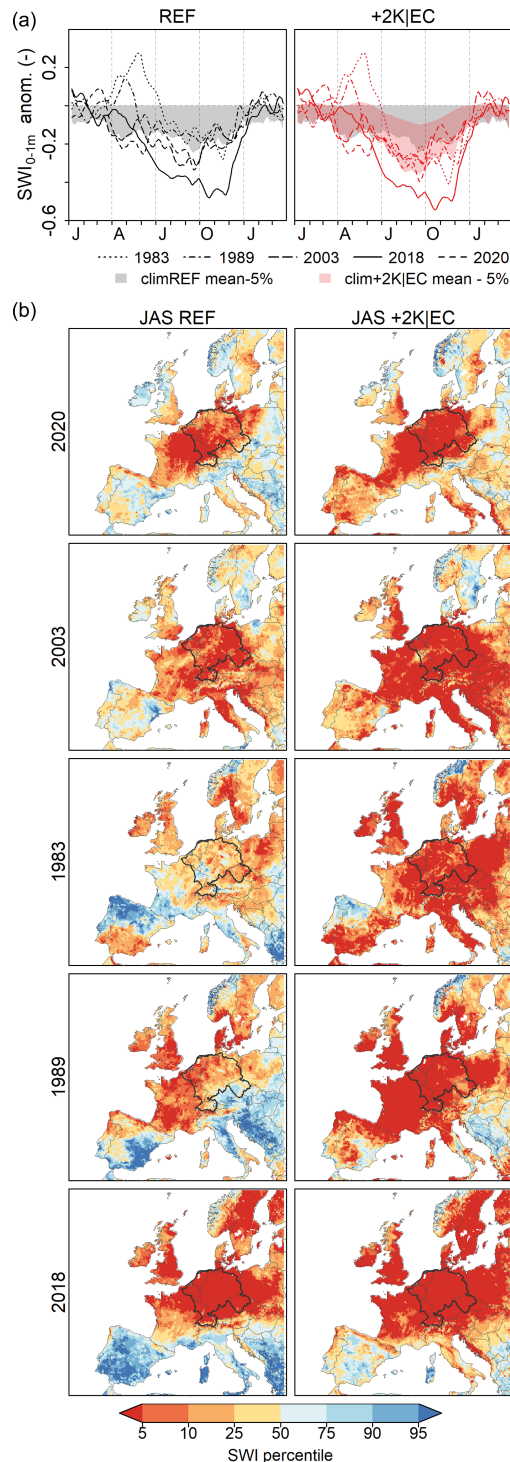
Figure 7. Present-day and future analogues of the top five future droughts, all exceeding the severity of the present-day 2003 drought in the west-central European river basins under +2K|EC. **(a)** Annual cycle of the SWI anomaly for present-day (left) and +2 °C conditions (right) (as in Fig. 5a). **(b)** Spatial structure of the top five droughts in JAS, showing the JAS-mean SWI percentile with respect to the 1980–2017 period (climREF). Droughts are shown in the order of increasing basin-mean drought severity under 2 °C warming. Dark-red colors indicate severe drought conditions.
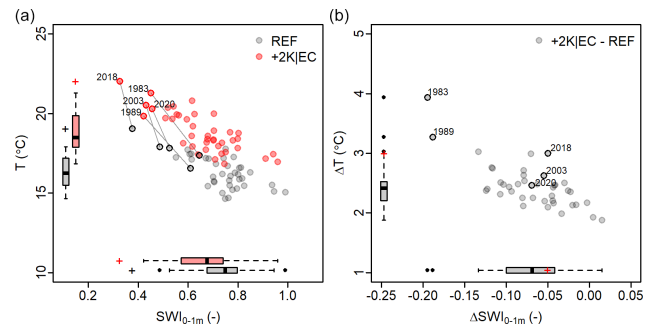
Figure 8. Scatterplot of the 1980–2020 JAS basin-mean near-surface temperature and SWI response. **(a)** Absolute values under present-day (grey) and +2 °C (red) conditions and their distribution (boxplots). **(b)** Response to 2 °C warming and its distribution (boxplots). Results are based on the EC-perturbed simulations. 2018 is indicated with + in the boxplots. The top five future droughts under 2 °C warming are marked.

6 Discussion

We have examined the implications of global warming for future droughts in west-central Europe, by employing PGW experiments for the 1980–2020 period. The simulations performed in this study allow for a systematic examination of the impact of global warming on droughts by comparing future drought analogues with present-day events, and the simulations provide anecdotal examples of the impact of global warming to complement conventional approaches based on large-ensemble climate simulations. Where the conventional approaches generate probabilistic estimates of changes in climate events, the PGW approach generates storylines of plausible future climate events that we can relate to. Storylines make future climate risks more tangible and more communicable than statistics (Hazeleger et al., 2015; Shepherd et al., 2018).

In the following we compare our results with studies based on large-ensemble simulations and discuss the implications of our findings.

6.1 The future 2018 drought: drier, hotter and bigger

It is generally hypothesized that under globally warmer conditions droughts set in earlier, last longer and are more intense if conditions favoring a drought occur (Trenberth et al., 2014; Seneviratne et al., 2010). Under the anomalously persistent atmospheric blocking conditions of 2018, global warming leads to increases in precipitation in early spring that (partially) compensate the increase in evaporation, limiting an earlier drought onset, while precipitation increases in autumn terminate the 2018 drought episode at the same time as under present-day conditions. However, the drought intensity indeed increases, yielding a 20 % (EC) to 39 % (HAD) increase in drought severity under 2 °C global warming. From an impact perspective, this is a considerable in-

crease, with substantial costs to society and nature already under present-day conditions (Van Hussen et al., 2019; De Brito et al., 2020; Toreti et al., 2019; Schuldt et al., 2020; Beillouin et al., 2020; Senf and Seidl, 2021). The increase in drought severity in summer co-occurs with an increase in local summer temperature that is considerably larger than the mean climate response. The combination of increasing heat and drought leads to even stronger increases in stress on nature and society and may enhance tree mortality (Allen et al., 2010), wildfire risk (Krikken et al., 2021), crop yield losses (Matiu et al., 2017) and water quality deterioration (Wolff and Van Vliet, 2021; Van Vliet et al., 2011), impacting ecosystems, industry, and energy and drinking water production. Moreover, the increase in drought extent under global warming, which also emerges in conventional ensemble simulations (e.g., Hari et al., 2020; Samaniego et al., 2018), implies that much larger parts of Europe will be affected simultaneously.

While the 2018 soil moisture response is considerable in an absolute sense, the soil moisture drying is small compared to the climatological response to 2 °C global warming. The same applies for 2003, the second largest drought episode in the 1980–2020 simulation period. While this has the physical explanation that the soil moisture response in drought years is limited by the strongly moisture-constrained conditions, this behavior may in part be explained as a PGW artifact. Extreme climate events occur when extreme drivers compound. In order for an event to become more extreme under PGW, all, or at least most, drivers of the event must be "pushed" towards a more extreme state by the perturbations. This is very likely for temperature under the strong temperature perturbation, yet it is not so obvious for, e.g., atmospheric stability and wind direction. Since there is a larger number of pathways for any other year to become more extreme, it is also statistically more likely that years in which moderately dry present-day conditions prevail show a much stronger drying response than the extreme 2018 drought and become more similar to the 2018 event under PGW.

More extreme drought occurrences than the 2018+2K event are plausible in a globally warmer world, in particular through an increase in drought duration driven by even more persistent or longer sequences of atmospheric blocking conditions, drier antecedent winter and spring conditions, and/or stronger climate-induced spring precipitation decreases than derived from the PGW experiments. Van der Wiel et al. (2021) also follow a storyline approach but sample drought events from a very large ensemble of transient global climate model simulations (EC-EARTH) that match or exceed the 2018 drought conditions in the Rhine basin under present-day and globally warmer conditions. They indeed find a set of events with a slightly stronger drying response in spring than under PGW with EC perturbations, but results are similar to the HAD perturbations. This is an elegant approach to find future analogues of present-day events as well, but such an approach relies on a very large GCM

(RCM) ensemble, and the atmospheric circulation of the future analogues does not necessarily match the present-day circulation, so a one-to-one comparison of present-day and future events is not possible.

6.2 The future of historic summers: moderately dry summers respond more strongly than extremes

The climatological-mean soil moisture drying response under PGW closely resembles results based on ensembles of transient climate model simulations. However, soils are generally replenished to present-day (near-saturation) soil moisture levels in winter under PGW, whereas, e.g., Ruosteenoja et al. (2018) and Van der Linden et al. (2019) find a small drying response throughout winter in transient simulations. This discrepancy could be explained by differences in GCM/RCM structure and model resolution. Also, the absence of high-frequency changes in the large-scale atmospheric circulation under PGW can explain these differences. Brogli et al. (2019) compare the full climate change response in transient simulations with the response under PGW and show that the high-frequency changes contribute to an increase in evaporative demand and decrease in precipitation in west-central European summer and to a reduction in the mean precipitation increase in winter. The "error" we make by neglecting these changes is likely small (De Vries et al., 2022) but may lead to a slight underestimation of mean soil moisture drying and moderate drought occurrences.

The increase in severe drought occurrences under PGW is in the range of changes in the drought intensity–frequency distribution derived from transient climate model simulations, with a doubling of 2003-like soil moisture droughts under 3 °C warming found by Samaniego et al. (2018) and 2018-like drought conditions (SPEI, standardized precipitation evapotranspiration index) becoming the new normal within the second half of the 21st century according to Toreti et al. (2019). The increase under PGW occurs under the historic large-scale atmospheric circulation, i.e., independently of changes in the frequency of atmospheric blocking conditions, and is owing to particularly strong soil moisture and temperature responses in years with moderately dry present-day conditions. While the transition from energy-limited to moisture-limited evaporation regimes can explain the co-occurrence of strong temperature increases and soil moisture drying, the relative contribution of different mechanisms that cause these strong responses varies widely and obscures a general picture. The results are robust with respect to the selected GCM to derive the perturbations.

The increase in frequency of extreme drought occurrences implies shorter recovery times between events, amplifying the impacts (Zscheischler et al., 2020). In particular, ecosystems can exhibit increased vulnerability to a second compared to an initial drought (Anderegg et al., 2020; Bastos et al., 2021). Temporally compounding financial losses may af-

fect for example the agricultural sector and industries with supply chains that depend on inland shipping.

6.3 Climate adaptation studies

The exploration of future analogues of historic (extreme) events is useful for different applications addressing climate process understanding, impact assessment or stress testing of climate adaptation strategies (Shepherd et al., 2018; Sillmann et al., 2021). The PGW simulations presented here have been used to investigate the hydrological impact of land use change and ecosystem adaptation to climate change, by forcing a hydrological model with time-variant vegetation parameters with the PGW simulations (Bouaziz et al., 2022). Bouaziz et al. (2022) show that increases in rooting depth in response to climate change result in enhanced evaporation and decreases in river runoff. It would be interesting to examine the impact of the hydrological changes on the meteorological and soil moisture drought development, which is in principle feasible in the PGW setup.

7 Conclusions

Droughts and associated heat waves form a threat to society and nature, as demonstrated in recent years in west-central Europe and presently again by the 2022 drought affecting large parts of Europe. To develop adaptation strategies, information about changes in drought risk under ongoing global warming is required. In this study we have examined the implications of global warming for future drought severity in west-central Europe, by systematically perturbing the 1980–2020 period towards future climate conditions using the pseudo global warming (PGW) approach. The reference experiment has been carried out with the RCM KNMI-RACMO2 forced by large-scale information from the ERA5 reanalysis. The PGW experiments use monthly-mean changes in temperature, humidity and winds derived from GCM projections. In this approach, the signal-to-noise ratio of the climate response is optimized and changes in droughts can be directly related to events and their societal impact in the recent history. Therewith the experiments provide tangible examples of what global warming entails and may serve as a tool to examine and communicate adaptation strategies.

Under 2 °C warming almost all years in the 1980–2020 period show a decrease in soil moisture availability in (spring,) summer and autumn, consistent with results based on transient climate model simulations. Under the circulation of 2018 the temperature response is strongly amplified, while the soil moisture response is limited by the strong moisture-constrained evaporation during present-day conditions. Nevertheless, the soil moisture deficit volume increases by 20 % to 39 % under 2 °C global warming, depending on the perturbing GCM, owing to an increase in drought intensity. The drought duration is barely impacted owing to increasing precipitation in spring, autumn and winter.

We furthermore show that the response in soil moisture drying and temperature can be particularly large for years with moderately dry conditions in the present-day climate. This implies that years that went hardly noticed in the present-day climate may emerge as very dry and hot years in a warmer world. Using present-day thresholds, the drought frequency strongly increases under 2 °C warming, with deficit volumes more severe than those of 2003 occurring every 8 years and exhibiting strongly enhanced temperatures. This shows that even without taking into account changes in the frequency of atmospheric blocking conditions, the drought risk in west-central Europe is strongly enhanced by the drought intensification and increase in frequency, yielding shorter recovery time between events for nature and society.

Appendix A: Simulations

Table A1. Characteristics of the ERA5 reanalysis forcing and GCM ensembles that have been used to derive the perturbations for the PGW simulations. T_{glob} refers to the annual global-mean 2 m temperature in the reference period 1991–2020. Mean is the ensemble-mean temperature; the standard deviation (SD) measures the inter-annual variability.

Reanalysis/GCM	Members	Horizontal resolution	T_{glob} in 1990–2020		Reference
		(long, lat)	mean (°C)	SD (°C)	
ERA5	–	0.250° × 0.250°	14.4	0.21	Hersbach et al. (2020)
EC-EARTH v2.3	r1i1p1 – 16i1p1	1.125° × 1.125°	13.6	0.28	Hazeleger et al. (2012)
HadGEM2-ES	r1i1p1 – r4i1p1	1.875° × 1.250°	14.5	0.39	Collins et al. (2011)
MPI-ES-LR	r1i1p1 – r3i1p1	1.870° × 1.875°	14.3	0.28	Giorgetta et al. (2013)

Table A2. Perturbation and greenhouse gas (GHG) forcing periods for the PGW simulations. The warming period is the period in which the target warming level is reached in the GCM simulations and is used to determine the perturbations. The PGW simulations are forced with projected aerosol and greenhouse gas concentrations for the years shown under GHG forcing.

GCM	Warming periods			GHG forcing			
	+1.5 °C	+2 °C	+3 °C	2018+1.5 °C	2018+2 °C	2018+3 °C	clim+2 °C
EC-EARTH v2.3	2037–2066	2048–2077	2069–2098	2058–2060	2069–2071	2090–2092	2030–2068
HadGEM2-ES	2027–2056	2036–2065	2053–2082	2048–2050	2057–2059	2074–2076	2018–2056
MPI-ES-LR	2036–2065	2048–2077	2068–2097	2036–2065	2069–2071	2089–2090	2030–2068
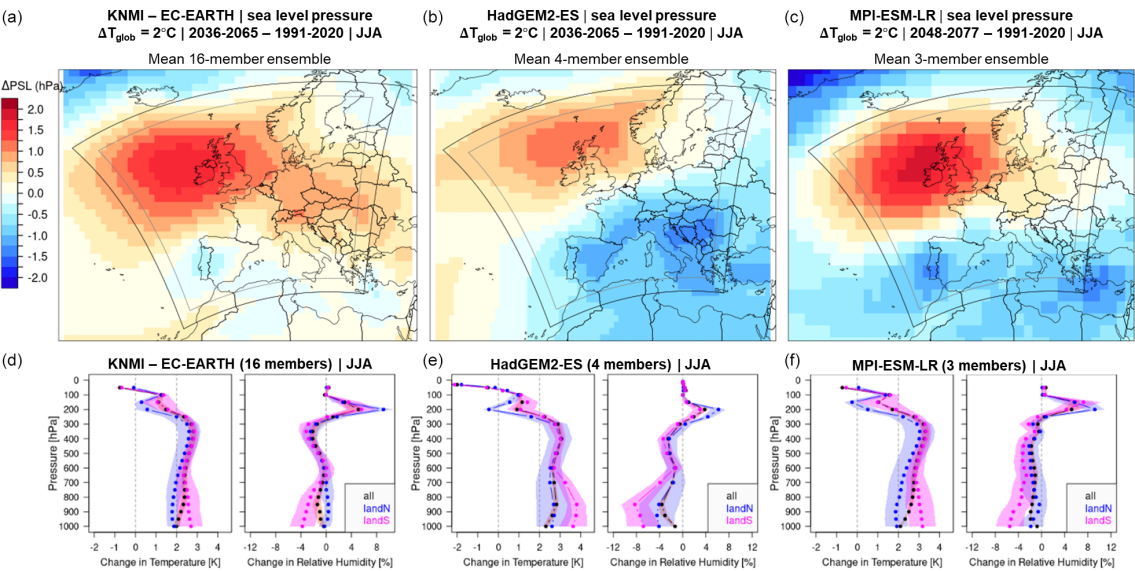
Figure A1. (a–c) Surface pressure perturbations corresponding to 2 °C global warming derived from **(a)** EC-EARTH, **(b)** HadGEM2 and **(c)** MPI for JJA (June–August). **(d–f)** Vertical profiles of temperature and relative humidity derived from the same GCMs. "All" refers to all grid cells enveloped by the solid line indicating the edges of the RCM domain; "landN" refers to land points north of 50° N; "landS" to cells in between 35 and 50° N. The shading indicates the spread across the regions. PSL: mean sea level pressure.

Appendix B: Atmospheric evaporative demand

The computation of soil evaporation and transpiration in HT-ESSEL both use a resistance approach (ECMWF, 2009) (see Eq. B1).

$$E = \frac{\rho_a}{r_a + r_i}[q_L - q_{sat}(T_{skin})], \quad\quad\quad (B1)$$

where r_i is the surface resistance, r_a is the aerodynamic resistance, ρ_a is the air density, q_L is the specific humidity of the lowest atmospheric model level and q_{sat} is the saturated specific humidity at skin temperature (T_{skin}). r_i is replaced by a canopy resistance (r_c) for transpiration and by a soil resistance (r_{soil}) for soil evaporation. r_c is modeled following Jarvis (1976) and is a function of the minimum stomatal resistance ($r_{S,min}$), the leaf area index (LAI), the downward short-wave radiation (R_s), unfrozen root soil water ($f_{liq\theta}$) and atmospheric water vapor deficit (D_a) (Eq. B2). The r_{soil} is a function of a minimum soil resistance ($r_{soil,min}$) and unfrozen soil water content in the top layer (f_{liq,θ_1}) (Eq. B3).

$$r_c = \frac{r_{S,min}}{LAI} \cdot f_1(R_s) \cdot f_2(f_{liq,\theta}) \cdot f_3(D_a) \quad\quad\quad (B2)$$

$$r_{soil} = r_{soil,min} \cdot f_2(f_{liq,\theta_1}) \quad\quad\quad (B3)$$

f_1, f_2 and f_3 are 1 for unconstrained conditions and larger than 1 for constrained conditions (see ECMWF, 2009). In order to determine the potential evaporation, f_2 for soil evaporation and transpiration and f_3 for transpiration are set to 1, while f_1 and all other variables (e.g., temperature, humidity) are taken from the prognostic computation with actual evaporation.

Appendix C: Present-day simulations and evaluation
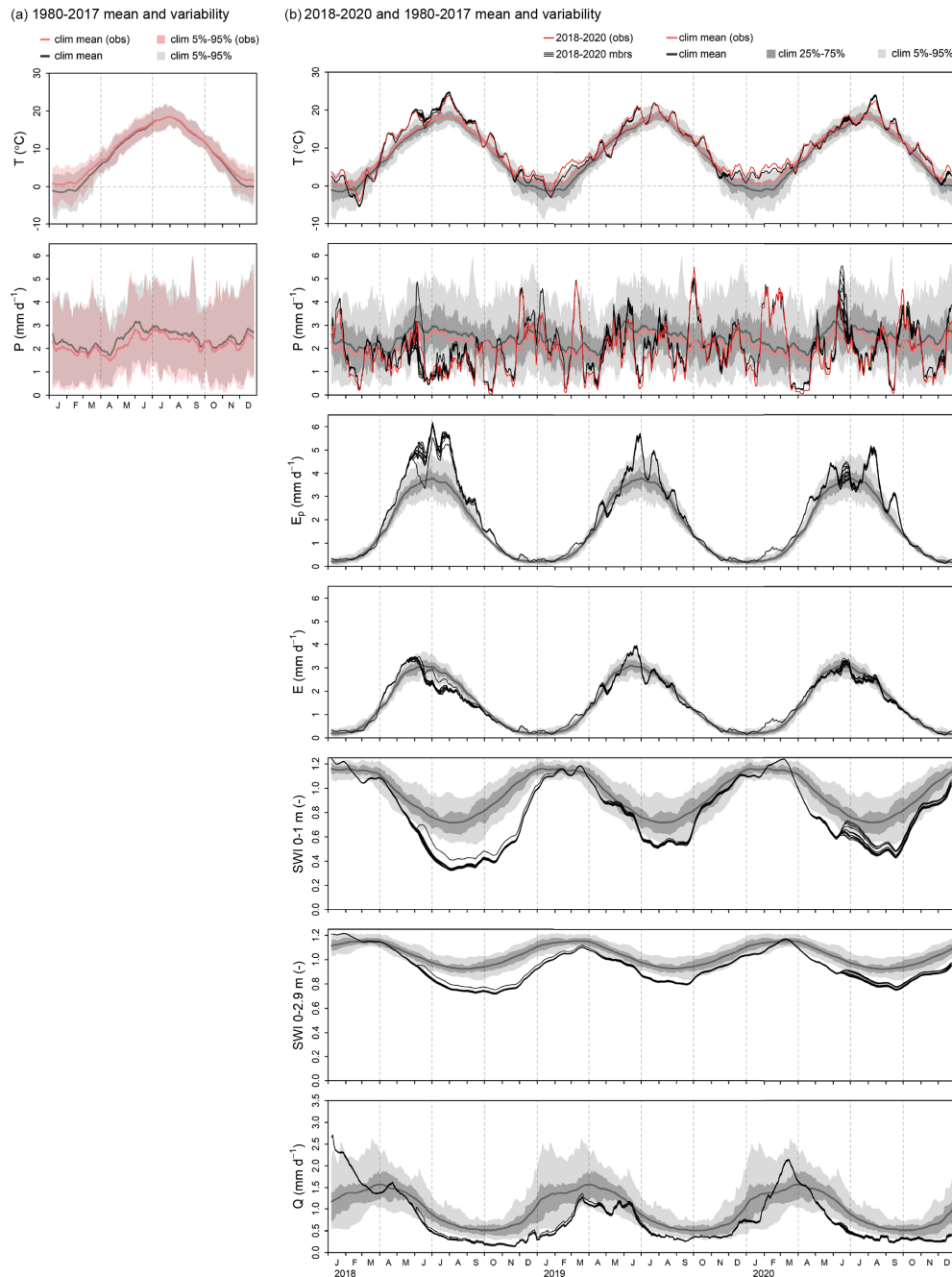
Figure C1. Basin-mean time series of **(a)** the 1980–2017 mean (lines) and 5th–95th percentile (shading) near-surface temperature (T) and precipitation (P) in observations (E-OBS v20.0, red) and simulations (climREF, grey) and **(b)** observed T and P and simulated $T\,P$, (potential) evaporation ($E_{(p)}$), the soil wetness index in the top 1 m ($SWI_{0-1\,m}$) and in all soil layers ($SWI_{0-2.9\,m}$), and runoff (Q) from 1 March 2018 to 31 December 2020. Black lines in **(b)** show the individual ensemble members of the simulated time series (2018REF); the red line depicts the observations (E-OBS v20.0 (2018) and v25.0 (2019–2020)). The simulated 1980–2017 mean and 25th–75th and 5th–95th percentiles are indicated by the thick grey line and grey shading. All time series are smoothed with a 14 d running mean.

Appendix D: Response

D1   Climate response
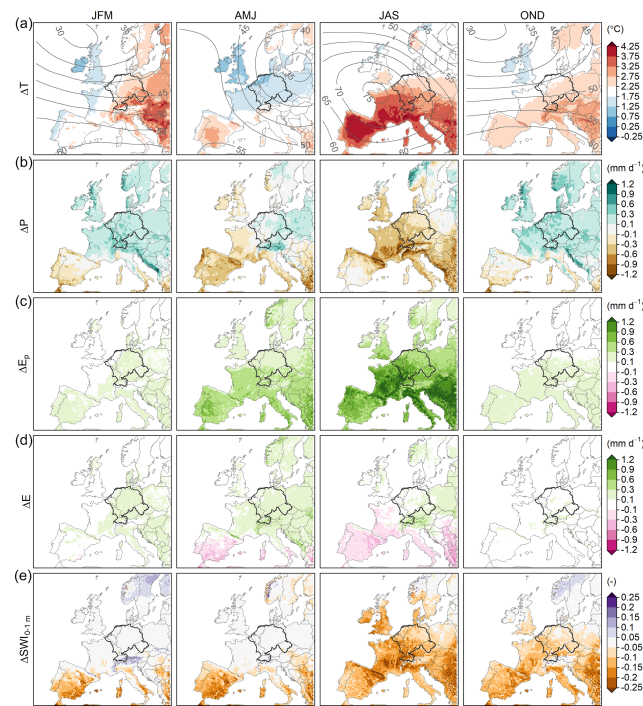
Figure D1. As Fig. 2 but for clim+2K|MPI.
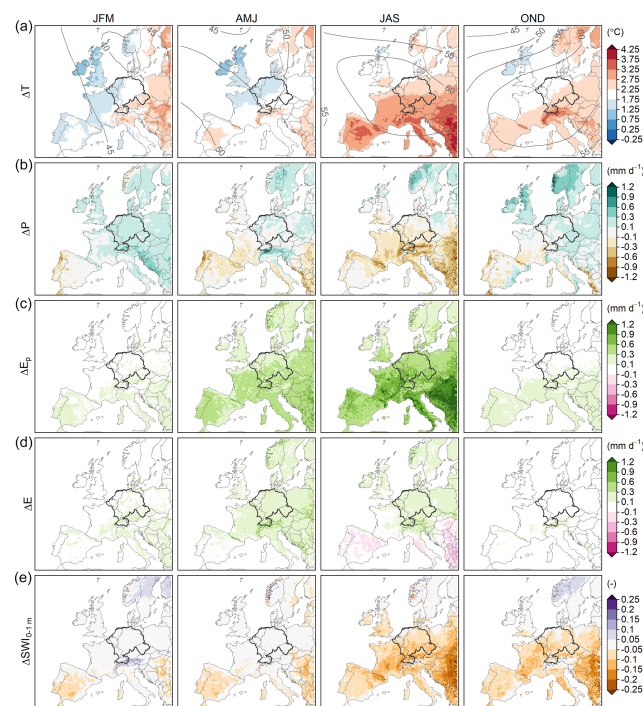
Figure D2. As Fig. 2 but for clim+2K|Had.

D2   2018 response
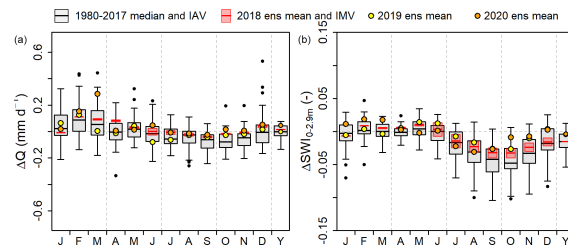
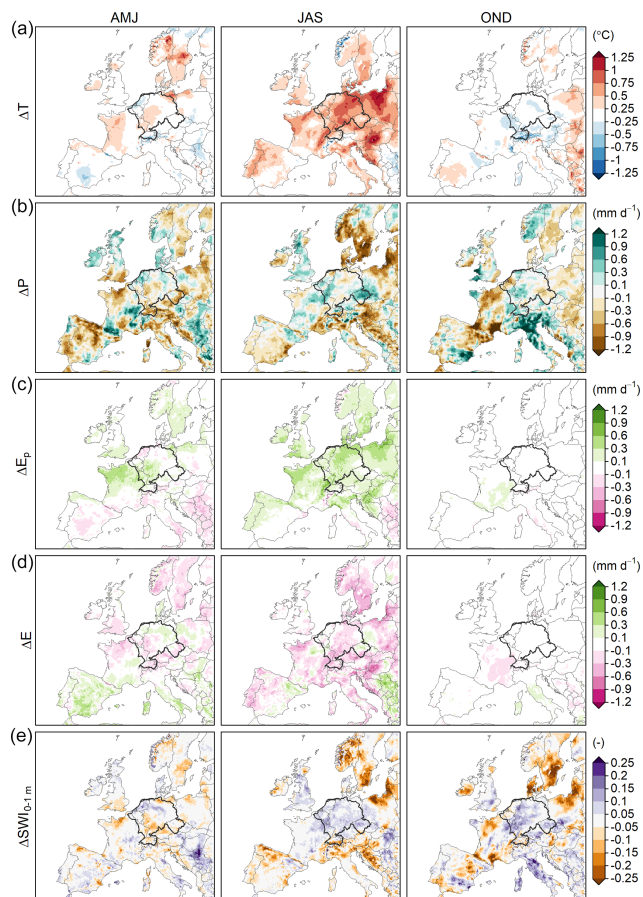
Figure D3. Extension of Fig. 3, with **(a)** runoff (Q) and **(b)** the soil wetness index in all soil layers ($SWI_{0-2.9\,m}$).
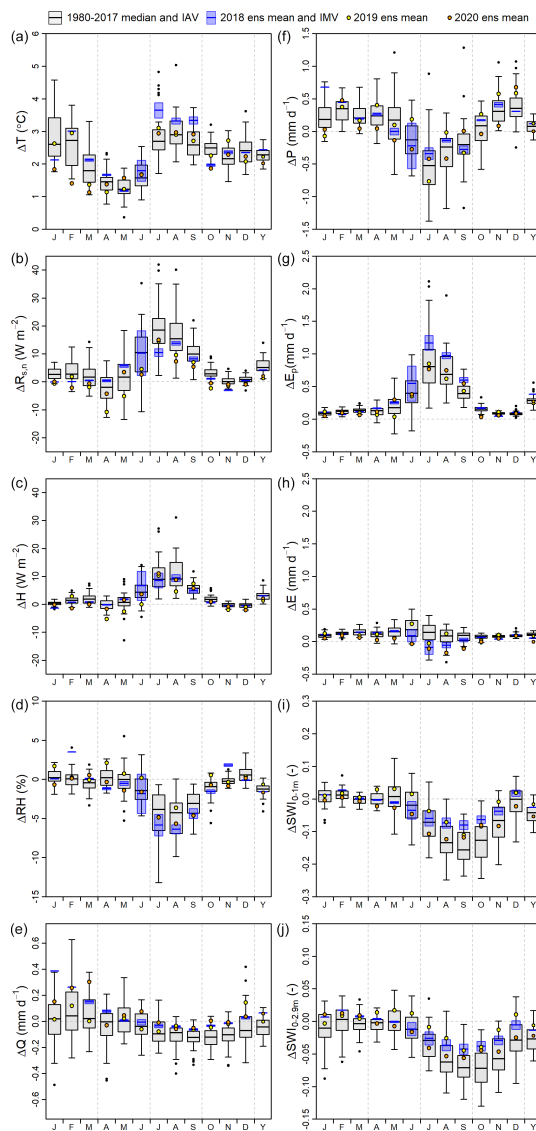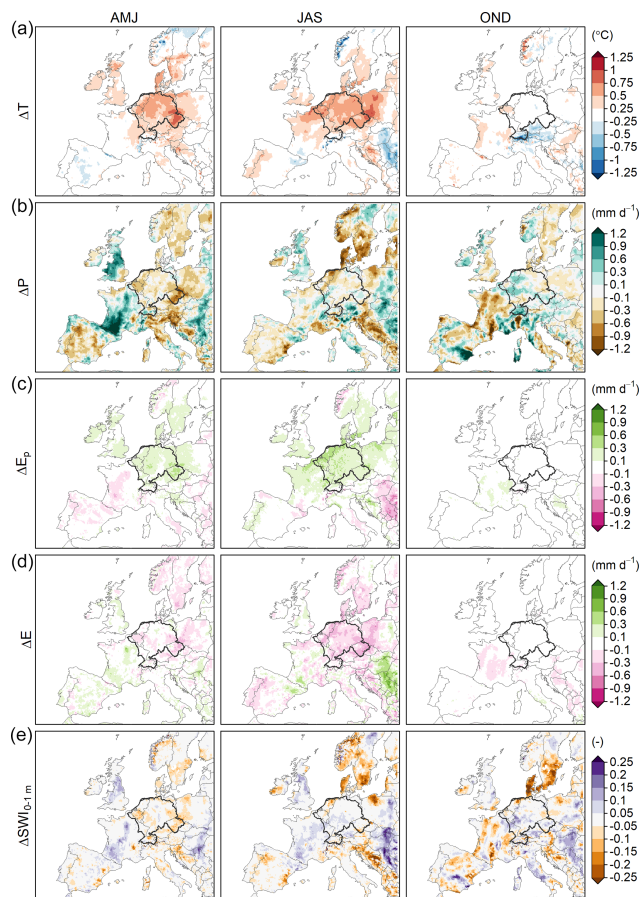

Figure D4. As Fig. 3 for clim+2K|MPI but extended with Q and $SWI_{0-2.9\,m}$. Note that the scale in **(e)** and **(j)** differs from the scale in **(f–h)** and **(i)** respectively, for visibility.
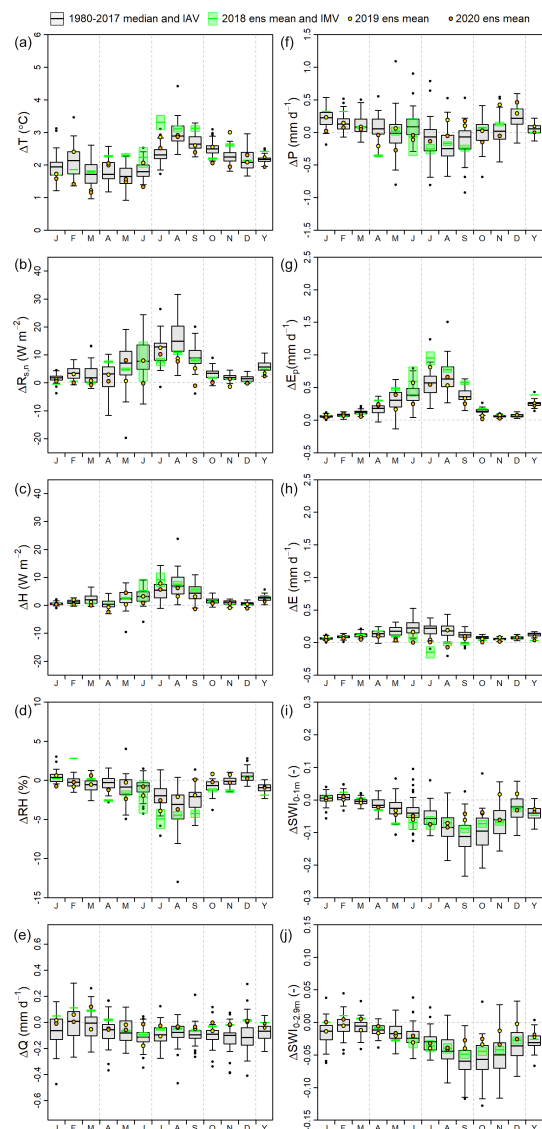
Figure D5. As Fig. D4 but for clim+2K|HAD.

Figure D6. As Fig. 4 but for clim+2K|MPI.

**Figure D7.** As Fig. 4 but for clim+2K|HAD.

D3 Impact on drought severity and frequency

Table D1. Drought severity of the 2018 drought for present-day conditions (REF) and for 1.5, 2 and 3 °C global warming. Listed are the ensemble mean and standard deviation (in parentheses).

		Duration (d)		Intensity (mm)		Deficit volume (mm d)	
	REF	233	(11)	36	(3)	8392	(968)
EC	+1.5 °C	229	(12)	42	(2)	9562	(810)
	+2 °C	228	(10)	44	(1)	10 049	(548)
	+3 °C	221	(11)	46	(1)	10 142	(614)
MPI	+1.5 °C	238	(1)	42	(1)	10 085	(359)
	+2 °C	238	(1)	44	(3)	10 497	(621)
	+3 °C	235	(1)	47	(2)	11 053	(538)
HAD	+1.5 °C	252	(1)	46	(2)	11 493	(606)
	+2 °C	251	(1)	46	(1)	11 646	(222)
	+3 °C	234	(20)	45	(3)	10 411	(770)
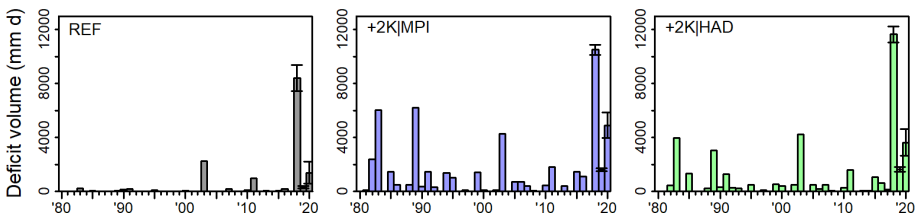
Figure D8. As Fig. 6a but for the MPI- and HAD-perturbed simulations.
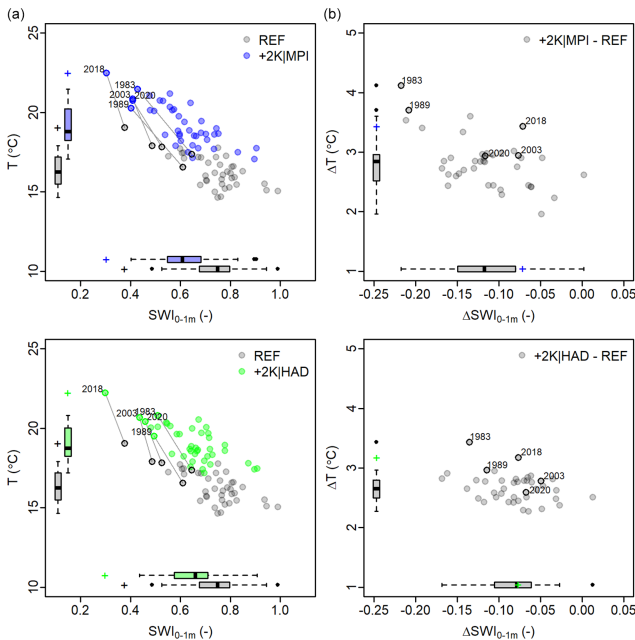
Figure D9. As Fig. 8 but for the MPI- and HAD-perturbed simulations.

Author contributions. All authors were involved in the study design. EEA carried out the analyses and prepared the manuscript. Results were discussed with all co-authors, and all co-authors commented extensively on early drafts. EvM performed all RCM simulations and prepared the perturbations together with HdV.

References

Aalbers, E. E., Lenderink, G., van Meijgaard, E., and van den Hurk, B. J. J. M.: Local-scale changes in mean and heavy precipitation in western Europe: climate change or internal variability?, Clim. Dynam., 50, 4745–4766, 2018.

Allen, C. D., Macalady, A. K., Chenchouni, H., Bachelet, D., Mcdowell, N., Vennetier, M., Kitzberger, T., Rigling, A., Breshears, D. D., and Hogg, E. H.: A global overview of drought and heat-induced tree mortality reveals emerging climate change risks for forests, Forest Ecol. Manag., 259, 660–684, https://doi.org/10.1016/j.foreco.2009.09.001, 2010.

Anderegg, W. R., Trugman, A. T., Badgley, G., Konings, A. G., and Shaw, J.: Divergent forest sensitivity to repeated extreme droughts, Nat. Clim. Change, 10, 1091–1095, https://doi.org/10.1038/s41558-020-00919-1, 2020.

Attema, J. J., Loriaux, J. M., and Lenderink, G.: Extreme precipitation response to climate perturbations in an atmospheric mesoscale model, ERL, 9, 014003, https://doi.org/10.1088/1748-9326/9/1/014003, 2014.

Balsamo, G., Beljaars, A., Scipal, K., Viterbo, P., Van den Hurk, B., Hirschi, M., and Betts, A. K.: A revised hydrology for the ECMWF model: Verification from field site to terrestrial water storage and impact in the integrated forecast system, J. Hydrometeorol., 10, 623–643, https://doi.org/10.1175/2008JHM1068.1, 2009.

Bundesanstalt für Gewässerkunde (BfG), Niedrigwasser-Berichtsperiode 12.–18.08.2022. Niedrigwasserextreme mit Aussicht auf zeitweise Linderung, https://www.bafg.de/DE/07_Nachrichten/220623_nw_download9.pdf?_blob=publicationFile, last access: 5 September 2022.

Bastos, A., Orth, R., Reichstein, M., Ciais, P., Viovy, N., Zaehle, S., Anthoni, P., Arneth, A., Gentine, P., Joetzjer, E., Lienert, S., Loughran, T., McGuire, P. C., O, S., Pongratz, J., and Sitch, S.: Vulnerability of European ecosystems to two compound dry and hot summers in 2018 and 2019, Earth Syst. Dynam., 12, 1015–1035, https://doi.org/10.5194/esd-12-1015-2021, 2021.

Beillouin, D., Schauberger, B., Bastos, A., Ciais, P., and Makowski, D.: Impact of extreme weather conditions on European crop production in 2018, Philos. T. R. Soc. B, 375, 20190510, https://doi.org/10.1098/rstb.2019.0510, 2020.

Benedict, I., Van Heerwaarden, C. C., Van der Linden, E. C., Weerts, A. H., and Hazeleger, W.: Anomalous moisture sources of the Rhine basin during the extremely dry summers of 2003 and 2018, Weather Clim. Extremes, 31, 100302, https://doi.org/10.1016/j.wace.2020.100302, 2021.

Bissolli. P. (Ed.): Europe and the Middle East [in "State of the Climate in 2018"], B. Am. Meteorol. Soc., 100, S217–S230, https://doi.org/10.1175/2019BAMSStateoftheClimate.1, 2019.

Bissolli. P. (Ed.): Europe and the Middle East [in "State of the Climate in 2019"], B. Am. Meteorol. Soc., 101, S363–S372, https://doi.org/10.1175/2020BAMSStateoftheClimate.1, 2020.

Bissolli, P. (Ed.): Europe and the Middle East [in "State of the Climate in 2020"], B. Am. Meteorol. Soc., 102, S410–S413, https://doi.org/10.1175/2021BAMSStateoftheClimate.1, 2021.

Bouaziz, L. J. E., Aalbers, E. E., Weerts, A. H., Hegnauer, M., Buiteveld, H., Lammersen, R., Stam, J., Sprokkereef, E., Savenije, H. H. G., and Hrachowitz, M.: Ecosystem adaptation to climate change: the sensitivity of hydrological predictions to time-dynamic model parameters, Hydrol. Earth Syst. Sci., 26, 1295–1318, https://doi.org/10.5194/hess-26-1295-2022, 2022.

Brakkee, E., van Huijgevoort, M. H. J., and Bartholomeus, R. P.: Improved understanding of regional groundwater drought development through time series modelling: the 2018–2019 drought in the Netherlands, Hydrol. Earth Syst. Sci., 26, 551–569, https://doi.org/10.5194/hess-26-551-2022, 2022.

Brogli, R., Sørland, S. L., Kröner, N., and Schär, C.: Causes of future Mediterranean precipitation decline depend on the season,

Environ. Res. Lett., 14, 114017, https://doi.org/10.1088/1748-9326/ab4438, 2019.

Brunner, M. I., Liechti, K., and Zappa, M.: Extremeness of recent drought events in Switzerland: dependence on variable and return period choice, Nat. Hazards Earth Syst. Sci., 19, 2311–2323, https://doi.org/10.5194/nhess-19-2311-2019, 2019.

Collins, W. J., Bellouin, N., Doutriaux-Boucher, M., Gedney, N., Halloran, P., Hinton, T., Hughes, J., Jones, C. D., Joshi, M., Liddicoat, S., Martin, G., O'Connor, F., Rae, J., Senior, C., Sitch, S., Totterdell, I., Wiltshire, A., and Woodward, S.: Development and evaluation of an Earth-System model – HadGEM2, Geosci. Model Dev., 4, 1051–1075, https://doi.org/10.5194/gmd-4-1051-2011, 2011.

Collins, M., Knutti, R., Arblaster, J., Dufresne, J.-L., Fichefet, T., Friedlingstein, P., Gao, X., Gutowski, W. J., Johns, T., Krinner, G., Shongwe, M., Tebaldi, C., Weaver, A. J., and Wehner, M.: Long-term Climate Change: Projections, Commitments and Irreversibility, in: Climate Change 2013: The Physical Science Basis. Contribution of Working Group I to the Fifth Assessment Report of the Intergovernmental Panel on Climate Change, edited by: Stocker, T. F., Qin, D., Plattner, G.-K., Tignor, M., Allen, S. K., Boschung, J., Nauels, A., Xia, Y., Bex, V., and Midgley, P. M., Cambridge University Press, Cambridge, United Kingdom and New York, NY, USA, 1029–1136, 2013.

Coppola, E., Nogherotto, R., Ciarlo', J. M., Giorgi, F., Van Meijgaard, E., Kadygrov, N., Iles, C., Corre, L., Sandstad, M., Somot, S., Nabat, P., Vautard, R., Levavasseur, G., Schwingshackl, C., Sillmann, J., Kjellström, E., Nikulin, G., Aalbers, E., Lenderink, G., Christensen, O. B., Boberg, F., Sørland, S. L., Demory, M.-E., Bülow, K., Teichmann, C., Warrach-Sagi, K., and Wulfmeyer, V.: Assessment of the European climate projections as simulated by the large EURO-CORDEX regional and global climate model ensemble, J. Geophys. Res.-Atmos., 126, e2019JD032356, https://doi.org/10.1029/2019JD032356, 2021.

Cornes, R. C., Van der Schrier, G., Van den Besselaar, E. J., and Jones, P. D.: An ensemble version of the E-OBS temperature and precipitation data sets, J. Geophys. Res.-Atmos., 123, 9391–9409, https://doi.org/10.1029/2017JD028200, 2018.

Coumou, D., Petoukhov, V., Rahmstorf, S., Petri, S., and Schellnhuber, H. J.: Quasi-resonant circulation regimes and hemispheric synchronization of extreme weather in boreal summer, P. Natl. Acad. Sci. USA, 111, 12331–12336, 2014.

De Brito, M. M., Kuhlicke, C., and Marx, A.: Near-real-time drought impact assessment: a text mining approach on the 2018/19 drought in Germany, Environ. Res. Lett., 15, 1040a9, https://doi.org/10.1088/1748-9326/aba4ca, 2020.

Deser, C., Phillips, A., Bourdette, V., and Teng, H. Uncertainty in climate change projections: the role of internal variability, Clim. Dynam., 38, 527–546, 2010.

De Vries, H., Lenderink, G., Van der Wiel, K., and Van Meijgaard, E.: Quantifying the role of the large-scale circulation on European summer precipitation change, Clim. Dynam., 59, 2871–2886, https://doi.org/10.1007/s00382-022-06250-z, 2022.

ECMWF: IFS Documentation CY33R1 – Part IV: Physical Processes, Number 4 in IFS Documentation. ECMWF, 2009, https://doi.org/10.21957/8o7vwlbdr, Operational implementation 3 June 2008, 2009.

Fischer, E., Sedláček, J., Hawkins, E., and Knutti, R.: Models agree on forced response pattern of precipitation and temperature extremes, Geophys. Res. Lett., 41, 8554–8562, 2014.

Fischer, E. M., Seneviratne, S. I., Vidale, P. L., Lüthi, D., and Schär, C.: Soil moisture-atmosphere interactions during the 2003 European summer heat wave, J. Climate, 20, 5081–5099, 2007.

Giorgetta, M. A., Jungclaus, J., Reick, C. H., Legutke, S., Bader, J., Böttinger, M., Brovkin, V., Crueger, T., Esch, M., Fieg, K., Glushak, K., Gayler, V., Haak, H., Hollweg, H.-D., Ilyina, T., Kinne, S., Kornblueh, L., Matei, D., Mauritsen, T., Mikolajewicz, U., Mueller, W., Notz, D., Pithan, F., Raddatz, T., Rast, S., Redler, R., Roeckner, E., Schmidt, H., Schnur, R., Segschneider, J., Six, K. D., Stockhause, M., Timmreck, C., Wegner, J., Widmann, H., Wieners, K.-H., Claussen, M., Marotzke, J., and Stevens, B.: Climate and carbon cycle changes from 1850 to 2100 in MPI-ESM simulations for the coupled model intercomparison project phase 5, J. Adv. Model. Earth Syst., 5, 572–597, https://doi.org/10.1002/jame.20038, 2013.

Gudmundsson, L. and Seneviratne, S. I.: Anthropogenic climate change affects meteorological drought risk in Europe, Environ. Res. Lett., 11, 044005, https://doi.org/10.1088/1748-9326/11/4/044005, 2016.

Gutiérrez, J. M., Jones, R. G., Narisma, G. T., Alves, L. M., Amjad, M., Gorodetskaya, I. V., Grose, M., Klutse, N. A. B., Krakovska, S., Li, J., Martínez-Castro, D., Mearns, L. O., Mernild, S. H., Ngo-Duc, T., Van den Hurk, B., and Yoon, J.-H.: Atlas. In Climate Change 2021: The Physical Science Basis, Contribution of Working Group I to the Sixth Assessment Report of the Intergovernmental Panel on Climate Change, edited by: Masson-Delmotte, V., Zhai, P., Pirani, A., Connors, S. L., Péan, C., Berger, S., Caud, N., Chen, Y., Goldfarb, L., Gomis, M. I., Huang, M., Leitzell, K., Lonnoy, E., Matthews, J. B. R., Maycock, T. K., Waterfield, T., Yelekçi, O., Yu, R., and Zhou, B., Cambridge University Press, Cambridge, United Kingdom and New York, NY, USA, 1927–2058, IPCC AR6 Atlas, 2021.

Hanel, M., Rakovec, O., Markonis, Y., Máca, P., Samaniego, L., Kysel?, J., and Kumar, R.: Revisiting the recent European droughts from a long-term perspective, Sci. Rep., 8, 1–11, https://doi.org/10.1038/s41598-018-27464-4, 2018.

Hari, V., Rakovec, O., Markonis, Y., Hanel, M., and Kumar, R.: Increased future occurrences of the exceptional 2018–2019 central European drought under global warming, Sci. Rep., 10, 1–10, https://doi.org/10.1038/s41598-020-68872-9, 2020.

Hazeleger, W., Severijns, C., Semmler, T., Ştefanescu, S., Yang, S., Wang, X., Wyser, K., Dutra, E., Baldasano, J. M., Bintanja, R., Bougeault, P., Caballero, R., Ekman, A. M. L., Christensen, J. H., van den Hurk, B., Jimenez, P., Jones, C., Kaållberg, P., Koenigk, T., McGrath, R., Miranda, P., van Noije, T., Palmer, T., Parodi, J. A., Schmith, T., Selten, F., Storelvmo, T., Sterl, A., Tapamo, H., Vancoppenolle, M., Viterbo, P., and Willeìn, U.: EC-Earth: a seamless earth-system prediction approach in action, B. Am. Meteorol. Soc., 91, 1357–1363, https://doi.org/10.1175/2010BAMS2877.1, 2010.

Hazeleger, W., Van den Hurk, B., Min, E., Van Oldenborgh, G. J., Petersen, A. C., Stainforth, D. A., Vasileiadou, E., and Smith, L. A.: Tales of future weather, Nat. Clim. Change, 5, 107–113, https://doi.org/10.1038/nclimate2450, 2015.

Hersbach, H., Bell, B., Berrisford, P., Hirahara, S., Horányi, A., Muñoz-Sabater, J., Nicolas, J., Peubey, C., Radu, R., Schepers,

https://doi.org/10.5194/nhess-23-1921-2023

Nat. Hazards Earth Syst. Sci., 23, 1921–1946, 2023

D., Simmons, A., Soci, C., Abdalla, S., Abellan, X., Balsamo, G., Bechtold, P., Biavati, G., Bidlot, J., Bonavita, M, De Chiara, G., Dahlgren, P., Dee, D., Diamantakis, M., Dragani, R., Flemming, J., Forbes, R., Fuentes, M., Geer, A., Haimberger, L., Healy, S., Hogan, R. J., Hólm, E., Janisková, M., Keeley, S., Laloyaux, P., Lopez, P., Lupu, C., Radnoti, G., De Rosnay, P., Rozum, I., Vamborg, F., Villaume, S., and Thépaut J.-N.: The ERA5 global reanalysis, Q. J. Roy. Meteorol. Soc., 146 1999–2049, 2020.

Jacob, D., Petersen, J., Eggert, B., Alias, A., Christensen, O. B., Bouwer, L. M., Braun, A., Colette, A., Déqué, M., Georgievski, G., Georgopoulou, E., Gobiet, A., Menut, L., Nikulin, G., Haensler, A., Hempelmann, N., Jones, C., Keuler, K., Kovats, S., Kröner, N., Kotlarski, S., Kriegsmann, A., Martin, E., Van Meijgaard, E., Moseley, C., Pfeifer, S., Preuschmann, S., Radermacher, C., Radtke, K., Rechid, D., Rounsevell, M., Samuelsson, P., Somot, S., Soussana, J.-F., Teichmann, C., Valentini, R., Vautard, R., Weber, B., and Yiou, P.: Euro-CORDEX: new high-resolution climate change projections for European impact research, Reg. Environ. Change, 14, 563–578, https://doi.org/10.1007/s10113-013-04, 2014.

Jarvis. P.: The interpretation of the variations in leaf water potential and stomatal conductance found in canopies in the field, Philos. T. Roy. Soc. A, Biological Sciences, 273, 593–610, 1976.

Klein Tank, A., Beersma, J., Bessembinder, J., van den Hurk, B. and Lenderink, G.: KNMI'14 climate scenarios for the Netherlands: A guide for professionals in climate adaptation, KNMI, De Bilt, The Netherlands, 34 pp., 2015

Kornhuber, K., Osprey, S., Coumou, D., Petri, S., Petoukhov, V., Rahmstorf, S., and Gray, L.: Extreme weather events in early summer 2018 connected by a recurrent hemispheric wave-7 pattern, Environ. Res. Lett., 14, 054002, https://doi.org/10.1088/1748-9326/ab13bf, 2019.

Kramer, N., Mens, M., Beersma, J., and Kielen, N.: Hoe extreem was de droogte van 2018?, H20-Online, https://www.h2owaternetwerk.nl/vakartikelen/hoe-extreem-was-de-droogte-van-2018 (last access: 18 May 2023), 2019.

Krikken, F., Lehner, F., Haustein, K., Drobyshev, I., and van Oldenborgh, G. J.: Attribution of the role of climate change in the forest fires in Sweden 2018, Nat. Hazards Earth Syst. Sci., 21, 2169–2179, https://doi.org/10.5194/nhess-21-2169-2021, 2021.

Kröner, N., Kotlarski, S., Fischer, E., Lüthi, D., Zubler, E., and Schär, C.: Separating climate change signals into thermodynamic, lapse-rate and circulation effects: theory and application to the European summer climate, Clim. Dynam., 48, 3415–3440, https://doi.org/10.1007/s00382-016-3276-3, 2017.

Lenderink, G. and Attema, J.: A simple scaling approach to produce climate scenarios of local precipitation extremes for the Netherlands, Environ. Res. Lett., 10, 085001, https://doi.org/10.1088/1748-9326/10/8/085001, 2015.

Lenderink, G., Van Ulden, A., Van den Hurk, B., and Van Meijgaard, E.: Summertime inter-annual temperature variability in an ensemble of regional model simulations: analysis of the surface energy budget, Clim. Change, 81, 233–247, https://doi.org/10.1007/s10584-006-9229-9, 2007.

Lenderink, G., Belušić, D., Fowler, H. J., Kjellström, E., Lind, P., Van Meijgaard, E., Van Ulft, B., and De Vries, H.: Systematic increases in the thermodynamic response of hourly precipitation extremes in an idealized warming experiment with a

convection-permitting climate model, Environ. Res. Lett., 14, 074012, https://doi.org/10.1088/1748-9326/ab214a, 2019.

Lenderink, G., De Vries, H., Van Meijgaard, E., Van der Wiel, K., and Selten, F.: A perfect model study on the reliability of the added small-scale information in regional climate change projections. Clim. Dynam., 60, 2563–2579, https://doi.org/10.1007/s00382-022-06451-6, 2023.

Manning, C., Widmann, M., Bevacqua, E., Van Loon, A. F., Maraun, D., and Vrac, M.: Increased probability of compound long-duration dry and hot events in Europe during summer (1950–2013), Environ. Res. Lett., 14,094006, https://doi.org/10.1088/1748-9326/ab23bf, 2019.

Matiu, M., Ankerst, D. P., and Menzel, A.: Interactions between temperature and drought in global and regional crop yield variability during 1961–2014, PLoS ONE, 12, e0178339, https://doi.org/10.1371/journal.pone.0178339, 2017.

Morice, C. P., Kennedy, J. J., Rayner, N. A., Winn, J. P., Hogan, E., Killick, R. E., Dunn, R. J. H., Osborn, T. J., Jones, P. D., and Simpson, I. R.: An updated assessment of near-surface temperature change from 1850: the HadCRUT5 dataset, J. Geophys. Res.-Atmos., 126, e2019JD032361, https://doi.org/10.1029/2019JD032361, 2021.

Orth, R., Zscheischler, J., and Seneviratne, S. I.: Record dry summer in 2015 challenges precipitation projections in central Europe, Sci. Rep., 6, 1–8, https://doi.org/10.1038/srep28334, 2016.

Padrón, R. S., Gudmundsson, L., Decharme, B., Ducharne, A., Lawrence, D. M., Mao, J., Peano, D., Krinner, G., Kim, H., and Seneviratne, S. I.: Observed changes in dry-season water availability attributed to human-induced climate change, Nat. Geosci., 13, 477–481, 2020.

Philip, S. Y., Kew, S. F., Van der Wiel, K., Wanders, N., and Van Oldenborgh, G. J.: Regional differentiation in climate change induced drought trends in the Netherlands, Environ. Res. Lett., 15, 081, https://doi.org/10.1088/1748-9326/ab97ca, 2020.

Prein, A. F., Rasmussen, R. M., Ikeda, K., Liu, C., Clark, M. P., and Holland, G. J.: The future intensification of hourly precipitation extremes, Nat. Clim. Change, 7, 48–52, https://doi.org/10.1038/nclimate3168, 2017.

Rakovec, O., Samaniego, L., Hari, V., Markonis, Y., Moravec, V., Thober, S., Hanel, M., and Kumar, R.: The 2018–2020 Multi-Year Drought Sets a New Benchmark in Europe, Earth's Future, 10, e2021EF002394m https://doi.org/10.1029/2021EF002394, 2022.

Rasmijn, L. M., Van der Schrier, G., Bintanja, R., Barkmeijer, J., Sterl, A., and Hazeleger W.: Future equivalent of 2010 Russian heatwave instensified by weakening soil moisture constraints, Nat. Clim. Change, 8, 381–385, https://doi.org/10.1038/s41558-018-0114-0

Rebetez, M., Mayer, H., Dupont, O., Schindler, D., Gartner, K., Kropp, J. P., and Menzel, A.: Heat and drought 2003 in Europe: a climate synthesis, Ann. Forest Sci., 63, 569–577, 2006.

Rösner, B., Benedict, I., Van Heerwaarden, C., Weerts, A., Hazeleger, W., Bissolli, P., and Trachte, K.: Sidebar 7.3: The long heat wave and drought in Europe in 2018 [in "state of the climate in 2018"], B. Am. Meteorol. Soc., 100, S221–S237, https://doi.org/10.1175/2019BAMSStateoftheClimate.1, 2019.

Ruosteenoja, K., Markkanen, T., Venäläinen, A., Räisänen, P., and Peltola, H.: Seasonal soil moisture and drought occurrence in Europe in CMIP5 projections for the 21st century, Clim. Dy-

Nat. Hazards Earth Syst. Sci., 23, 1921–1946, 2023

https://doi.org/10.5194/nhess-23-1921-2023

nam., 50, 1177–1192, https://doi.org/10.1007/s00382-017-3671-4, 2018.

Samaniego, L., Thober, S., Kumar, R., Wanders, N., Rakovec, O., Pan, M., Zink, M., Sheffield, J., Wood, E. F., and Marx. A.: Anthropogenic warming exacerbates European soil moisture droughts, Nat. Clim. Change, 8, 421–426, 2018.

Schär, C., Frei, C., Lüthi, D., and Davies, H. C.: Surrogate climate-change scenarios for regional climate models, Geophys. Res. Lett., 23, 669–672, 1996.

Schär, C., Vidale, P. L., Lüthi, D., Frei, C., Häberli, C., Liniger, M. A., and Appenzeller, C.: The role of increasing temperature variability in European summer heatwaves, Nature, 427, 332–336, 2004.

Schuldt, B., Buras, A., Arend, M., Vitasse, Y., Beierkuhnlein, C., Damm, A., Gharun, M., Grams, T. E., Hauck, M., Hajek, P., Hartmann, H., Hiltbrunner, E., Hoch, G., Holloway-Phillips, M., Körner, C., Larysch, E., Lübbe, T., Nelson, D. B., Ramming, A., Rigling, A., Rose, L., Ruehr, N. K., Schumann, K., Weiser, F., Werner, C., Wohlgemuth, T., Zang, C. S., and Kahmen, A.: A first assessment of the impact of the extreme 2018 summer drought on central European forests, Basic Appl. Ecol., 45, 86–103, https://doi.org/10.1016/j.baae.2020.04.003, 2020.

Selten, F. M., Bintanja, R., Vautard, R., and Van den Hurk, B.: Future continental summer warming constrained by the present-day seasonal cycle of surface hydrology, Sci. Rep., 10, 1–7, 2020.

Seneviratne, S., Corti, T., Davin, E. L., Hirschi, M., Jaeger, E. B., Lehner, I., Orlowsky, B., and Teuling, A. J.: Investigating soil moisture–climate interactions in a changing climate: A review, Earth-Sci. Rev., 99, 125–161, 2010.

Seneviratne, S.I., Nicholls, N., Easterling, D., Goodess, C.M., Kanae S., Kossin, J., Luo, Y., Marengo, J., McInnes, K., Rahimi, M., Reichstein, M., Sorteberg, A., Vera, C., and Zhang, X.: Changes in climate extremes and their impacts on the natural physical environment, in: Managing the Risks of Extreme Events and Disasters to Advance Climate Change Adaptation, edited by: Field, C. B., Barros, V., Stocker, T. F., Qin, D., Dokken, D. J., Ebi, K. L., Mastrandrea, M. D., Mach, K. J., Plattner, G.-K., Allen, S. K., Tignor, M., and Midgley, P. M.: A Special Report of Working Groups I and II of the Intergovernmental Panel on Climate Change (IPCC). Cambridge University Press, Cambridge, UK, and New York, NY, USA, 109–230, 2012.

Senf, C. and Seidl, R.: Persistent impacts of the 2018 drought on forest disturbance regimes in Europe, Biogeosciences, 18, 5223–5230, https://doi.org/10.5194/bg-18-5223-2021, 2021.

Shepherd, T. G.: Atmospheric circulation as a source of uncertainty in climate change projections, Nat. Geosci., 7, 703–708, 2014.

Shepherd, T. G.: Storyline approach to the construction of regional climate change information, P. Roy. Soc. A, 475 20190013, https://doi.org/10.1098/rspa.2019.0013, 2019.

Shepherd, T. G., Boyd, E., Calel, R. A., Chapman, S. C., Dessai, S., Dima-West, I. M., Fowler, H. J., James, R., Maraun, D., Martius, O., Senior, C. A., Sobel, A. H., Stainforth, D. A., Tett, S. F. B., Trenberth, K. E., Van den Hurk, B. J. J. M., Watkins, N. W., Wilby, R. L., and Zenghelis, D.: Storylines: An alternative approach to representing uncertainty in climate change, Clim. Change, 151, 555–571, https://doi.org/10.1007/s10584-018-2317-9, 2018.

Sillmann, J., Shepherd, T., Van den Hurk, B., Hazeleger, W., Romppainen-Martius O., and Zscheischler, J.: Event-based storylines to address climate risk, Earth's Future, 9, e2020EF001783, https://doi.org/10.1029/2020EF001783, 2021.

Sluijter, R., Plieger, M., Van Oldenborgh, G., Beersma, J., and De Vries, H.: De droogte van 2018: een analyse op basis van het potentiële neerslagtekort, Royal Netherlands Meteorological Institute, Tech. Rep., 117162, 38 pp., 2018.

Sousa, P. M., Trigo, R. M., Barriopedro, D., Soares, P. M., Ramos, A. M., and Liberato, M. L.: Responses of European precipitation distributions and regimes to different blocking locations, Clim. Dynam., 48, 1141–1160, 2017.

Sousa, P. M., Trigo, R. M., Barriopedro, D., Soares, P. M., and Santos, J. A.: European temperature responses to blocking and ridge regional patterns, Clim. Dynam., 50, 457–477, 2018.

Sousa, P. M., Barriopedro, D., García-Herrera, R., Ordóñez, C., Soares, P. M. M., and Trigo, R. M: Distinct influences of large-scale circulation and regional feedbacks in two exceptional 2019 European heatwaves, Commun. Earth Environ., 1, 48, https://doi.org/10.1038/s43247-020-00048-9, 2020.

Spinoni, J., Barbosa, P., De Jager, A., McCormick, N., Naumann, G., Vogt, J. V., Magni, D., Masante, D., and Mazzeschi, M.: A new global database of meteorological drought events from 1951 to 2016, J. Hydrol. Reg. Stud., 22, 100593, https://doi.org/10.1016/j.ejrh.2019.100593, 2019.

Stott, P. A., Stone, D. A., and Allen, M. R.: Human contribution to the European heatwave of 2003, Nature, 432, 610–614, 2004.

Taylor, K. E., Stouffer, R. J., and Meehl, G. A.: An overview of CMIP5 and the experiment design, B. Am. Meteorol. Soc., 93, 485–498, 2012.

Toreti, A., Belward, A., Perez-Dominguez, I., Naumann, G., Luterbacher, J., Cronie, O., Seguini, L., Manfron, G., Lopez-Lozano, R., Baruth, B., Van den Berg, M., Dentener, F., Ceglar, A., Chatzopoulos, T., and Zampieri, M.: The exceptional 2018 European water seesaw calls for action on adaptation, Earth's Future, 7, 652–663, 2019.

Toreti, A., Bavera, D., Acosta Navarro, J., Cammalleri, C., de Jager, A., Di Ciollo, C., Hrast Essenfelder, A., Maetens, W., Magni, D., Masante, D., Mazzeschi, M., Niemeyer, S., and Spinoni, J.: Drought in Europe August 2022, Publications Office of the European Union, Luxembourg, https://doi.org/10.2760/264241, JRC130493, 2022.

Trachte, K., Obregón, A., Bissolli, P., Kennedy, J. J., Parker, D. E., Trigo, R. M., and Barriopedr, D.: Europe [in "State of the Climate in 2011"], B. Am. Meteorol. Soc., 93, S186–S191, https://doi.org/10.1175/2019BAMSStateoftheClimate.1, 2012.

Trenberth, K. E., Dai, A., Van Der Schrier, G., Jones, P. D., Barichivich, J., Briffa, K. R., and Sheffield, J.: Global warming and changes in drought, Nat. Clim. Change, 4, 17–22, 2014.

van der Linden, E. C., Haarsma, R. J., and van der Schrier, G.: Impact of climate model resolution on soil moisture projections in central-western Europe, Hydrol. Earth Syst. Sci., 23, 191–206, https://doi.org/10.5194/hess-23-191-2019, 2019.

Van der Wiel, K., Lenderink, G., and De Vries, H.: Physical storylines of future European drought events like 2018 based on ensemble climate modelling, Weather and Climate Extremes, p. 100350, https://doi.org/10.1016/j.wace.2021.100350, 2021.

Van der Wiel, K., Batelaan, T. J., and Wanders, N.: Large increases of multi-year droughts in north-western Europe in a warmer climate, Clim. Dynam., 60, 1781–1800, https://doi.org/10.1007/s00382-022-06373-3, 2023,

https://doi.org/10.5194/nhess-23-1921-2023

Nat. Hazards Earth Syst. Sci., 23, 1921–1946, 2023

Van Garderen, L. and Mindlin, J.: A storyline attribution of the 2011/2012 drought in Southeastern South America, Weather, 77, 212–218, https://doi.org/10.1002/wea.4185, 2022.

Van Hussen, K., Van de Velde, I., Läkamp, R., Van der Kooij, S., and Hekman, A.: Economische schade door droogte in 2018. Ecorys, Rotterdam, Technical Report; 55 pp., 2019.

Van Meijgaard, E., Van Ulft, L., Lenderink, G., de Roode, S., Wipfler, E., Boers, R., and Van Timmermans, R.: Refinement and application of a regional atmospheric model for climate scenario calculations of western Europe, Technical Report KVR 054/12, 46 pp., ISBN/EAN 978-90-8815-046-3, 2012.

Van Vliet, M. T. H., Ludwig, F., Zwolsman, J. J. G., Weedon, G. P., and Kabat, P.: Global river temperatures and sensitivity to atmospheric warming and changes in river flow, Water Resour. Res., 47, W02544, https://doi.org/10.1029/2010WR009198, 2011.

Vautard, R., van Aalst, M., Boucher, O., et al.: Human contribution to the record-breaking June and July 2019 heatwaves in western Europe, Environ. Res. Lett., 15, 094077, https://doi.org/10.1088/1748-9326/aba3d4, 2020

Vogel, M. M., Zscheischler, J., and Seneviratne, S. I.: Varying soil moisture–atmosphere feedbacks explain divergent temperature extremes and precipitation projections in central Europe, Earth Syst. Dynam., 9, 1107–1125, https://doi.org/10.5194/esd-9-1107-2018, 2018.

Vogel, M. M., Zscheischler, J., Wartenburger, R., Dee, D., and Seneviratne, S. I.: Concurrent 2018 hot extremes across northern hemisphere due to human-induced climate change, Earth's future, 7, 692–703, 2019.

Wehrli, K., Hauser, M., and Seneviratne, S. I.: Storylines of the 2018 Northern Hemisphere heatwave at pre-industrial and higher global warming levels, Earth Syst. Dynam., 11, 855–873, https://doi.org/10.5194/esd-11-855-2020, 2020.

WMCN-LCW: Droogtemonitor, Rijkswaterstaat, Ministerie van Infrastructuur en Waterstaat, https://waterberichtgeving.rws.nl/owb/droogtemonitor, last access: 5 September 2022.

Wolff, E. and Van Vliet, M. T. H.: Impact of the 2018 drought on pharmaceutical concentrations and general water quality of the Rhine and Meuse rivers, STOTEN, 778, https://doi.org/10.1016/j.scitotenv.2021.146182, 2021.

Woollings, T., Barriopedro, D., Methven, J., Son, S.-W., Martius, O., Harvey, B., Sillmann, J., Lupo, A. R., and Seneviratne, S.: Blocking and its response to climate change, Curr. Clim. Change Rep., 4, 287–300, 2018.

Yevjevich, V.: An objective approach to definitions and investigations of continental hydrologic droughts, Hydrology Paper No. 23, Colorado State University, Fort Collins, CO, 18 pp., 1967.

Yiou, P., Cattiaux, J., Faranda, D., Kadygrov, N., Jézéquel, A., Naveau, P., Ribes, A., Robin, Y., Thao, S., Van Oldenborgh, G. J., and Vrac, M.: Analyses of the northern European summer heatwave of 2018, B. Am. Meteorol. Soc., 101, S35–S40, https://doi.org/10.1175/BAMS-D-19-0170.1, 2020

Zscheischler, J. and Fischer, E. M.: The record-breaking compound hot and dry 2018 growing season in Germany, Weather Clim. Extremes, 29, 100270, ISSN 2212-0947, https://doi.org/10.1016/j.wace.2020.100270, 2020.

Zscheischler, J. and Seneviratne, S. I.: Dependence of drivers affects risks associated with compound events, Sci. Adv., 3, e1700263, https://doi.org/10.1126/sciadv.1700263 2017.

Zscheischler, J., Martius, O., Westra, S., Bevacqua, E., Raymond, C., Horton, R. M., Van den Hurk, B., AghaKouchak, A., Jézéquel, A., Mahecha, M. D., Maraun, D., Ramos, A. M., Ridder, N. N., Thiery, W., and Vignotto, E.: A typology of compound weather and climate events, Nat. Rev. Earth Env., 1, 333–347, https://doi.org/10.1038/s43017-020-0060-z, 2020.